intermediate. If the anchoring process occurs in such a sterically orientated way that the protein offers binding sites which facilitate a shift of Mg^{2+}, either into an α,β position or to the γ group, an activation would result. There are indeed examples where the specific function of a divalent metal ion is the formation of an enzyme-metal ion-nucleotide bridged complex.[14,99]

This reasoning indicates that the anchoring process of a nucleotide to the enzyme-protein is crucial for an activation. As purine-nucleotides are much more easily anchored via stacking and hydrophobic interactions than pyrimidine-nucleotides, this difference may be the main reason why pyrimidine-NTPs, e.g., UTP, are not able to substitute effectively for ATP in many enzymic systems.[15,100]

From Figure 11 it is evident that the two activation "partners", e.g., the two metal ions, may interact not only in a M(α,β)-M-(γ)-like way (as is shown in the figure) but that a M(α)-M(β,γ) coordination can also be enforced and this would then lead to a reactive species ready for the transfer of either a nucleoside monophosphate or a diphosphate group. In fact the concept outlined allows selective activation for the transfer of all groups which can be derived from a nucleoside triphosphate, including the transfer of a nucleoside group.

Acknowledgment. We thank Ms. Rita Baumbusch for the skillful performance of experiments. The elemental analyses were kindly performed in the microanalytical laboratories of CIBA-GEIGY AG, Basel. The computers were made available by the Rechenzentrum der Universität Basel (Univac 1100/81). This support and research grants from the Swiss National Science Foundation (H.S.) and the support of the sabbatical leave of R.M.M. to the University of Basel through Boston University and by grants from the U.S. and Swiss National Science Foundations under the U.S.-Switzerland Cooperative Science Program are gratefully acknowledged.

Registry No. Dien, 111-40-0; Dpa, 1539-42-0; AMP, 61-19-8; IMP, 131-99-7; GMP, 85-32-5; ϵ-AMP, 37482-16-9; AMP·NO, 4061-78-3; ATP, 56-65-5; CTP, 65-47-4; TuMP, 16719-46-3; RiMP, 4300-28-1; Cu/ATP (1:1), 18925-86-5; Cd/ATP (2:1), 74114-69-5; Cd/ATP (1:1), 72052-13-2; Cd/CTP (1:1), 75898-71-4; Zn/ATP (1:1), 6602-83-1; Ni/ATP (1:1), 18839-84-4; Cu^{2+}(dien), 45520-77-2; Cu^{2+}(Dpa), 65956-54-9; Mg, 7439-95-4; Ni, 7440-02-0; Zn, 7440-66-6; Cd, 7440-43-9; adenosine, 58-61-7; L-tryptophan, 73-22-3.

Supplementary Material Available: Table S1 and Figures S1-S5 giving additional kinetic details (6 pages). Ordering information is given on any current masthead page.

(99) (a) Aull, J. L.; Daron, H. H.; Friedman, M. E.; Melius, P. *Met. Ions Biol. Syst.* **1980**, *11*, 337-376. (b) Koren, R.; Mildvan, A. S. *Biochemistry* **1977**, *16*, 241-249. (c) Bean, B. L.; Koren, R.; Mildvan, A. S. *Biochemistry* **1977**, *16*, 3322-3333.

(100) (a) Weinstock, G. M.; McEntee, K.; Lehman, I. R. *J. Biol. Chem.* **1981**, *256*, 8856-8858. (b) Gerhart, J. C.; Pardee, A. B. *J. Biol. Chem.* **1962**, *237*, 891-896.

Chain-Folding Initiation Structures in Ribonuclease A: Conformational Analysis of *trans*-Ac-Asn-Pro-Tyr-NHMe and *trans*-Ac-Tyr-Pro-Asn-NHMe in Water and in the Solid State

G. T. Montelione, E. Arnold, Y. C. Meinwald, E. R. Stimson, J. B. Denton, S.-G. Huang, J. Clardy, and H. A. Scheraga*

Contribution from the Baker Laboratory of Chemistry, Cornell University, Ithaca, New York 14853. *Received April 16, 1984*

Abstract: In order to investigate the role of β-bends with non-native *trans* peptide bonds preceding Pro^{114} and Pro^{93} in the mechanism of folding of bovine pancreatic ribonuclease A, we have examined the conformations of the synthetic peptides Ac-Asn-Pro-Tyr-NHMe (I) and Ac-Tyr-Pro-Asn-NHMe (II) in water and in the solid state. These sequences occur at residues 113-115 and 92-94, respectively, in ribonuclease A. Evidence for a significant population of I with a *trans*-Asn-Pro peptide bond and a β-bend at Pro-Tyr in water includes backbone/backbone and side chain/backbone NOE's, N-H bending frequencies characteristic of a β-bend, and hydrogen bonds detected by solvent spin-saturation transfer measurements involving the TyrN*H* and N*H*Me amide protons. Comparison of the Raman spectrum in water with that of the crystal suggests that the major backbone conformation in solution is similar to that in the solid state. Populations of II with a *trans*-Tyr-Pro peptide bond also have a hydrogen bond involving the N*H*Me amide. The crystal structure of I ($R \leq 0.064$), determined in two different crystalline forms, is a type I β-bend at Pro-Tyr with a *trans* peptide bond at Asn-Pro and intramolecular hydrogen bonds involving both the TyrN*H* and N*H*Me amide protons. The crystal structure of II ($R < 0.076$) also has a *trans* peptide bond (at Tyr-Pro), but an extended backbone conformation. The relevance of these results to the mechanism(s) of chain-folding initiation in ribonuclease A is discussed.

It is generally believed that local short- and medium-range interactions dominate in determining the native structure of globular proteins.[1-12] In the case of bovine pancreatic ribonuclease A, this principle is supported by the observations that reduced ribonuclease retains ~0.04% of native enzymatic activity[13] and ~6% native antigenic activity.[14] Spectroscopic measurements also demonstrate that the reduced protein,[15-17] the C-peptide

(1) Kotelchuck, D.; Scheraga, H. A. *Proc. Natl. Acad. Sci. U.S.A.* **1968**, *61*, 1163.
(2) Kotelchuck, D.; Scheraga, H. A. *Proc. Natl. Acad. Sci. U.S.A.* **1969**, *62*, 14.
(3) Ptitsyn, O. B. *Akad. Nauk SSSR, Dokl. Biophys.* **1973**, *210*, 87.
(4) Ponnuswamy, P. K.; Warme, P. K.; Scheraga, H. A. *Proc. Natl. Acad. Sci. U.S.A.* **1973**, *70*, 830.
(5) Scheraga, H. A. *Pure Appl. Chem.* **1973**, *36*, 1.
(6) Tanaka, S.; Scheraga, H. A. *Proc. Natl. Acad. Sci. U.S.A.* **1975**, *72*, 3802.
(7) Tanaka, S.; Scheraga, H. A. *Macromolecules* **1977**, *10*, 291.
(8) Matheson, R. R., Jr.; Scheraga, H. A. *Macromolecules* **1978**, *11*, 819.
(9) Némethy, G.; Scheraga, H. A. *Proc. Natl. Acad. Sci. U.S.A.* **1979**, *76*, 6050.
(10) Kanehisa, M. I.; Tsong, T. Y. *J. Mol. Biol.* **1978**, *124*, 177.
(11) Scheraga, H. A. In "Protein Folding"; Jaenicke, R., Ed.; Elsevier, Amsterdam, 1980; p 261.
(12) Ptitsyn, O. B.; Finkelstein, A. V. *Q. Rev. Biophys.* **1980**, *13*, 339.
(13) Garel, J. R. *J. Mol. Biol.* **1978**, *118*, 331.
(14) Chavez, L. G., Jr.; Scheraga, H. A. *Biochemistry* **1980**, *19*, 1005.

0002-7863/84/1506-7946$01.50/0

lactone fragment[18-20] (corresponding to the 13 N-terminal amino acid residues of ribonuclease), and the S-peptide fragment[20,21] (corresponding to the 20 N-terminal amino acid residues of ribonuclease A) adopt ordered backbone conformation(s) in water at particular temperatures and pH's. Presumably, such ordered structures, which are determined by local interactions under folding conditions, can play an important role in the formation of initial structural intermediates during the early stages of protein folding.

This, and the following paper,[22] are part of a series of studies designed to identify local structures that play a role in the *initial stages* of folding in ribonuclease A. We refer to these local structures, which are stabilized by short- and medium-range interactions *under folding conditions*, as chain-folding initiation structures. They are important in protein folding because they limit the conformational space accessible to the protein in the *initial stages* of folding, thereby directing subsequent folding events. The formation of a chain-folding initiation structure, however, need not represent the rate-limiting step in the folding process, nor need its conformation be exactly the same as that of the corresponding sequence in the native protein.

Assuming that reverse-turn structures stabilized by hydrophobic interactions are likely candidates for chain-folding "nucleation" sites, Matheson and Scheraga[8] used free energy calculations to identify residues Ile[106]-Val[118] as the most probable site of formation of initial structural intermediate(s). This hypothesis is supported by peptide fragment complementation studies[23] which indicate that the tryptic fragment 105–124 of ribonuclease A is an efficient inhibitor of folding. Other experimental studies, however, indicate that the antigenic site involving residues 80–104 is the first to form in the oxidative folding experiments[24] and the last to unfold in the thermal denaturation process.[25-27] From an examination of medium-range interresidue contacts in native ribonuclease A, Némethy and Scheraga[9] have identified residues 71–111 (referred to as site E) and residues 103–124 (referred to as site F), along with four other sequences, as likely sites for chain-folding initiation. These results suggest that chain-folding initiation may take place independently in more than one chain-folding initiation site in ribonuclease A. In this, and the following[22] paper, we have examined synthetic fragments of chain-folding initiation sites E and F corresponding to sequences with β-bend conformations in the native protein in order to determine to what extent local interactions stabilize β-bends in these two parts of the molecule under folding conditions.

In the crystal structure[28,29] of ribonuclease A, site F (residues[9] 103–124) forms part of a β-sheet structure with a type VI β-bend[30,31] at Asn[113]–Pro[114] (i.e., with a *cis*-peptide bond at Asn[113]-Pro[114]). Site E forms part of an *independent* β-sheet structure with a type III β-bend[30,31] at Gly[88]-Ser[89] and a type VI β-bend[26,27] at Tyr[92]-Pro[93] (i.e., with a *cis*-peptide bond at Tyr[92]-Pro[93]). These conformational features are represented in Figure 1, drawn with a simple computer graphics program.[32]

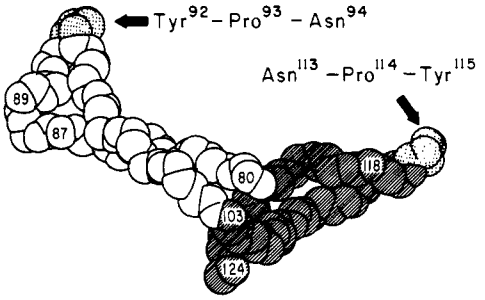

Figure 1. Computer graphics[32] representation of the backbone conformation of most of the β-sheet "hydrophobic core" of native ribonuclease A. The locations of β-bends at Asn[113]-Pro[114]-Tyr[115] and Tyr[92]-Pro[93]-Asn[94] (in chain-folding initiation sites F and E, respectively) are indicated by dotted atoms. Backbone atoms corresponding to residues 103–124 (site F) are represented by shaded atoms (except Asn[113]-Pro[114]-Tyr[115] which are dotted) and those corresponding to residues 80–102 (most of site E) by open atoms (except Tyr[92]-Pro[93]-Asn[94] which are dotted).

The striking symmetry of the amino acid sequence in the vicinity of the β-bend site of site F, Asn[113]-Pro[114]-Tyr[115], and around one of the β-bends in site E, Tyr[92]-Pro[93]-Asn[94], suggests a possible role for short-range interactions in Asn/Pro/Tyr that favor β-bend conformations which are essential in the *initial stages* of protein folding. Significantly, Pro-Tyr and Pro-Asn are found in β-bend conformations in the X-ray crystal structures of several other proteins[30,33] including porcine elastase, horse α-hemoglobin, midge larva hemoglobin, papain, and subtilisin. In concanavalin A,[34] Pro-Asn of Tyr-Pro-Asn occurs as a β-bend while Pro-Tyr of Asn-Pro-Tyr is in a bend conformation in bovine pancreatic phopholipase A_2.[35] In all these cases, the β-bend involves all *trans*-peptide bonds with proline in bend position[31] $i + 1$. In ribonuclease A,[28,29] however, type VI β-bends occur in both Asn-Pro-Tyr and Tyr-Pro-Asn, i.e. with a *cis*-X-Pro peptide bond and proline in bend position[31] $i + 2$.

While a recent investigation[36] demonstrates that the folding kinetics of disulfide-intact ribonuclease A can be simulated without assuming the presence of structural folding intermediates or non-native proline peptide bonds, many studies[37-41] support the contention[37] that ribonuclease A can fold to a metastable enzymatically active form which may have non-native (i.e., *trans*) peptide bonds at Asn[113]-Pro[114] and/or Tyr[92]-Pro[93]. Direct evidence for non-native peptide bond conformations in folding intermediates, however, is not available.

In a previous study of the peptide *cis/trans* conformational equilibrium of the terminally blocked peptides Ac-Asn-Pro-Tyr-NHMe and Ac-Tyr-Pro-Asn-NHMe in water[42] we presented preliminary evidence, based on chemical shift data and vicinal coupling constants, for ordered structure in one or both of these solvated peptides. Because open-chain peptides generally do not form β-bend structures in water, we have undertaken a more complete conformational analysis of these synthetic fragments of bovine pancreatic ribonuclease A. In this paper, we show that

(15) Schaffer, S. W. *Int. J. Peptide Protein Res.* **1975**, *7*, 179.
(16) Takahashi, S.; Kontani, T.; Yoneda, M.; Ooi, T. *J. Biochem.* **1977**, *82*, 1127.
(17) Swadesh, J. K.; Montelione, G. T.; Thannhauser, T. W.; Scheraga, H. A. *Proc. Natl. Acad. Sci. U.S.A.* **1984**, *81*, 4606.
(18) Brown, J. E.; Klee, W. A. *Biochemistry* **1971**, *10*, 470.
(19) Bierzynski, A.; Kim, P. S.; Baldwin, R. L. *Proc. Natl. Acad. Sci. U.S.A.* **1982**, *79*, 2470.
(20) Silverman, D. N.; Kotelchuck, D.; Taylor, G. T.; Scheraga, H. A. *Arch. Biochem. Biophys.* **1972**, *150*, 757.
(21) Kim, P. S.; Bierzynski, A.; Baldwin, R. L. *J. Mol. Biol.* **1982**, *162*, 187.
(22) Oka, M.; Montelione, G. T.; Scheraga, H. A. *J. Am. Chem. Soc.*, following paper in this issue.
(23) Carty, R. P.; Gerewitz, F.; Pincus, M. R. *Biophys. J.* **1982**, *37*, 95a.
(24) Chavez, L. G., Jr.; Scheraga, H. A. *Biochemistry* **1980**, *19*, 996.
(25) Burgess, A. W.; Scheraga, H. A. *J. Theor. Biol.* **1975**, *53*, 403.
(26) Ooi, T.; Rupley, J. A.; Scheraga, H. A. *Biochemistry* **1963**, *2*, 432.
(27) Bigelow, C. C. *J. Biol. Chem.* **1961**, *236*, 1706.
(28) Wlodawer, A.; Bott, R.; Sjölin, L. *J. Biol. Chem.* **1982**, *257*, 1325.
(29) Borkakoti, N.; Moss, D. S.; Palmer, R. A. *Acta Crystallogr., Sect. B* **1982**, *B38*, 2210.
(30) Lewis, P. N.; Momany, F. A.; Scheraga, H. A. *Biochim. Biophys. Acta* **1973**, *303*, 211.
(31) Chain reversals involving four residues may be characterized by the values of the dihedral angles ϕ_{i+1}, ψ_{i+1}, ϕ_{i+2}, ψ_{i+2}, where i is the index of the first residue on the amino terminal side of the bend sequence. Hence, only the second and third residues in the bend are designated to indicate its position in the amino acid sequence. The classification of β-bend types used here is described in ref 30.
(32) Zientara, G. P.; Nagy, J. A. *Comput. Chem.* **1983**, *7*, 67.
(33) Chou, P. Y.; Fasman, G. D. *J. Mol. Biol.* **1977**, *115*, 135.
(34) Reeke, G. N., Jr.; Becker, J. W.; Edelman, G. M. *J. Biol. Chem.* **1975**, *250*, 1525.
(35) Dijkstra, B. W.; Kalk, K. H.; Hol, W. G. J.; Drenth, J. *J. Mol. Biol.* **1981**, *147*, 97.
(36) Lin, L.-N.; Brandts, J. F. *Biochemistry* **1983**, *22*, 573.
(37) Cook, K. H.; Schmid, F. X.; Baldwin, R. L. *Proc. Natl. Acad. Sci. U.S.A.* **1979**, *76*, 6157.
(38) Schmid, F. X. *Eur. J. Biochem.* **1981**, *114*, 105.
(39) Schmid, F. X.; Blaschek, H. *Eur. J. Biochem.* **1981**, *114*, 111.
(40) Rehage, A.; Schmid, F. X. *Biochemistry* **1982**, *21*, 1499.
(41) Pincus, M. R.; Gerewitz, F.; Wako, H.; Scheraga, H. A. *J. Protein Chem.* **1983**, *2*, 131.
(42) Stimson, E. R.; Montelione, G. T.; Meinwald, Y. C.; Rudolph, R. K. E.; Scheraga, H. A. *Biochemistry* **1982**, *21*, 5252.

local interactions do, in fact, favor a β-bend conformation in water with non-native (*trans*) X-Pro peptide bonds in the Asn-Pro-Tyr sequence. A bend conformation of *trans*-Ac-Asn-Pro-Tyr-NHMe can also be crystallized from water. Furthermore, conformational energy calculations[22] indicate that the *cis* conformers of both Ac-Asn-Pro-Tyr-NHMe and Ac-Tyr-Pro-Asn-NHMe (present in solution at concentrations too low for experimental measurements) have an especially strong tendency to form β-bends. Therefore, on the basis of both experimental and theoretical[22] studies, both native (*cis*) and non-native (*trans*) Asn^{113}-Pro^{114} peptide bonds may be anticipated in early-forming folding intermediates with native-like reverse-turn structures. While β-bends are also favored for native (*cis*) Tyr-Pro peptide bonds[22] (at $Tyr\text{-}Pro^{31}$ of Tyr-Pro-Asn), short-range interactions do not favor formation of a β-bend at Tyr^{92}-Pro^{93}-Asn^{94} when the Tyr-Pro peptide bond is *trans*.

Experimental Section

Peptide Synthesis. The synthesis and characterization of the peptides Ac-Asn-Pro-NHMe, Ac-Pro-Tyr-NHMe, Ac-Asn-Pro-Tyr-NHMe, Ac-Tyr-Pro-NHMe, and Ac-Tyr-Pro-Asn-NHMe have been described previously.[42] Ac-Ala-Pro-Tyr-NHMe was prepared as follows. Boc-Ala-Pro-OH[43] (608 mg) was coupled with H-Tyr-$NHCH_3$·HCl (461 mg) by the *N,N'*-dicyclohexylcarbodiimide/1-hydroxybenzotriazole method. The product, Boc-Ala-Pro-Tyr-$NHCH_3$ (615 mg), was obtained as a foam from ethyl acetate (R_f 0.72; chloroform–methanol–acetic acid, 95:20:3). This material was deprotected with 5 N HCl/1,2-dimethoxyethane for 30 min at room temperature, and the resulting H-Ala-Pro-Tyr-$NHCH_3$·HCl was precipitated by addition of ether. Six hundered and six milligrams of this material was then acylated with a 1.5 molar excess of 4-nitrophenyl acetate by stirring in *N*-ethylmorpholine/dimethylformamide at room temperature for 24 h. The solvent was removed in vacuo and the oily residue was dissolved in water and washed with ethyl acetate. The aqueous layer was then chromatographed on a Dowex 50W-X2 (H^+ form) column with H_2O as the eluant to give 474 mg of Ac-Ala-Pro-Tyr-NHMe, as a foam (R_f 0.39, chloroform–methanol–acetic acid, 95:20:3). Several attempts to crystallize this hygroscopic product were unsuccessful. $[\alpha]_D$ −89.9° (*c* 0.5, MeOH). Amino acid analysis: Pro, 0.95; Ala, 1.01; Tyr, 1.04.

All peptides used in the study were analyzed by high-pressure liquid chromatography on a Spectra Physics SP8000 liquid-chromatography system using a reversed phase C_{18} column and were found to elute as single peaks (≳98%) using an H_2O/acetonitrile gradient and 210-nm detection. Homogeneity was also demonstrated by comparing the absorption and fluorescence properties of the tyrosine chromophore with that of Ac-Tyr-NHMe and by proton NMR spectroscopy. No evidence for racemization was observed in the NMR spectra of synthetic intermediates or products.

Extent of Aggregation. Freezing point depression measuremenets, using a cryoscope designed and built in our laboratory,[44] were made to determine the degree of aggregation of Ac-Asn-Pro-Tyr-NHMe at ~0 °C in H_2O. The molecular weight determined by this method was 500 ± 90 and 494 ± 20 at concentrations of 4 and 8 mg/mL, respectively. These values agree reasonably well with the theoretical value, 447, indicating little or no aggregation under these conditions. Ac-Tyr-Pro-Asn-NHMe was not sufficiently soluble near the freezing point of water for cryoscopic measurements. No dependence of the spectroscopic measurements on peptide concentrations in the range of 4–10 mg/mL were observed.

Proton NMR Measurements. Proton NMR spectra were recorded at 300 MHz on a Brüker WM-300 spectrometer. Data manipulation involved simple exponential smoothing of the free induction decay, corresponding to 0.1 Hz of line broadening. Proton NMR spectra of peptides in H_2O were obtained by using a tailored 2-1-4 excitation pulse,[45] with a null at the H_2O frequency, and constant phase detection. This pulse sequence circumvents the dynamic range problem associated with proton NMR measurements in H_2O solution. The probe temperature was maintained at 27 ± 1 °C in all measurements. Chemical shifts are expressed relative to δ_{HOD} = 4.80 ppm.

Nuclear Overhauser Effect (NOE) Measurements in H_2O. NOE measurements in H_2O, for identification of N*H*/N*H* NOE's, were made by selectively irradiating amide proton resonances with a weak 10-s pulse followed by a 3-ms homogeneity-spoil pulse (to randomize the coherence of the signal due to a small amount of nonselective irradiation of the H_2O protons), a 15-ms homogeneity recovery period, and a 2-1-4 Redfield tailored-pulse[45] with an excitation null at the H_2O resonance frequency. The amide proton irradiation was turned off and its frequency offset temporarily switched to an arbitrary off-resonance frequency during the homo-spoil and acquisition periods in order to avoid the effects of residual current in the coil which would otherwise generate a noise-spike at the amide proton irradiation frequency. With use of this pulse sequence, spectra with irradiation on- and off-resonance were alternately added and subtracted from memory, generating an NOE difference spectrum. Tests of the selectivity of the weak 10-s irradiation pulse at frequency δ demonstrated that there was <1% nonselective irradiation of resonances at δ ± 50 Hz. NOE's could be measured unambiguously for protons whose resonances were $|\Delta\delta| < 50$ Hz from the on-resonance irradiation frequency, δ, by setting the off-resonance irradiation at $\delta + 2\Delta\delta$ Hz. Control difference spectra (i.e., in the absence of NOE) obtained by using this technique with on-resonance irradiation of frequency δ revealed no perturbation (<0.1%) of the equilibrium spin distribution of protons with resonance frequencies at $\delta' = \delta \pm 20$ Hz.

Measurement of Backbone Peptide Proton Exchange Rates. Intramolecular hydrogen bonds in aqueous solution were identified by comparing pseudo-first-order rate constants for amide proton exchange in the synthetic peptides with those measured in the corresponding terminally blocked single amino acids. Amide proton assignments for these peptides in H_2O have been presented elsewhere.[42] The pseudo-first-order rate constants for amide proton exchange in H_2O were measured by the method of solvent spin-saturation transfer.[46-53] The theoretical basis for these measurements has been discussed elsewhere.[53-56]

For secondary (i.e., backbone) amides, the pseudo-first-order rate constant for proton exchange, k_{ex}, was calculated by assuming the high-mobility dynamic limit, in which conformational transitions between intramolecular and solvent hydrogen-bonded conformations are rapid relative to the rate of proton exchange. This assumption is justified by the monoexponential decay of spin-saturated states of hydrogen-bonded protons (as will be shown later in Figure 7). In the high-mobility dynamic limit the pseudo-first-order rate constant for backbone amide proton exchange (in the absence of solvent/solute NOE) is given by[54-56]

$$k_{ex} = \eta / T_{1,app} \quad (1)$$

where η is the fractional *decrease* in intensity of the amide proton magnetization under steady-state solvent saturation and $T_{1,app}$ is the apparent longitudinal relaxation time of the exchangable amide proton in H_2O.

The quantity η was obtained experimentally by comparing amide proton intensities in spectra obtained with decoupler irradiation centered at the H_2O resonance frequency (solvent saturated) with spectra recorded without solvent irradiation. The following pulse sequence was used to obtain solvent-saturated spectra. The H_2O solvent resonance was irradiated for 3 s after which the irradiation was switched off. Then, after a 1-ms instrumental delay, the spectrum of the amide and aromatic protons was obtained with a 2-1-4 Redfield tailored-pulse and a 1.8-s acquisition period. The total time between tailored-pulses, 4.8 s, was sufficiently long to ensure spin-relaxation of amide and aromatic protons. In order to obtain complete solvent saturation, 20 successive scans with this pulse sequence were carried out prior to data acquisition. Control measurements demonstrated that the solvent H_2O proton spin states were >99% saturated following the 1-ms instrumental delay when the 20 successive pre-equilibration scans were included. Fifty to five hundred free induction decays were summed and Fourier transformed for each spectrum.

(43) Lorenzi, G. P.; Doyle, B. B.; Blout, E. R. *Biochemistry* **1971**, *10*, 3046.
(44) Davenport, V. G.; Stimson, E. R.; Scheraga, H. A. *Anal. Biochem.*, in press.
(45) Redfield, A. G.; Kunz, S. D.; Ralph, E. K. *J. Magn. Reson.* **1975**, *19*, 114.
(46) Waelder, S.; Lee, L.; Redfield, A. G. *J. Am. Chem. Soc.* **1975**, *97*, 2927.
(47) Bleich, H. E.; Glasel, J. A. *J. Am. Chem. Soc.* **1975**, *97*, 6585.
(48) Waelder, S. F.; Redfield, A. G. *Biopolymers* **1977**, *16*, 623.
(49) Redfield, A. G.; Waelder, S. *J. Am. Chem. Soc.* **1979**, *101*, 6151.
(50) Krishna, N. R.; Huang, D. H.; Glickson, J. D.; Rowan, R.; Walter, R. *Biophys. J.* **1979**, *26*, 345.
(51) Lenkinski, R. E.; Stephens, R. L.; Krishna, N. R. *Biochemistry* **1981**, *20*, 3122.
(52) Krishna, N. R.; Huang, D.-H.; Vaughn, J. B., Jr.; Heavner, G. A.; Goldstein, G. *Biochemistry* **1981**, *20*, 3933.
(53) Krishna, N. R.; Sarathy, K. P.; Huang, D.-H.; Stephens, R. L.; Glickson, J. D.; Smith, C. W.; Walter, R. *J. Am. Chem. Soc.* **1982**, *104*, 5051.
(54) Campbell, I. D.; Dobson, C. M.; Ratcliffe, R. G. *J. Magn. Reson.* **1977**, *27*, 455.
(55) Campbell, I. D.; Dobson, C. M.; Ratcliffe, R. G.; Williams, R. J. P. *J. Magn. Reson.* **1978**, *29*, 397.
(56) Krishna, N. R.; Goldstein, G.; Glickson, J. D. *Biopolymers* **1980**, *19*, 2003.

In order to avoid the dynamic range problem associated with excitation of the H_2O protons in a broad-band relaxation-time measurement, we chose to measure the apparent longitudinal relaxation time, $T_{1,app}$, for each peptide or amide proton individually by the method of selective spin-saturation recovery. In these measurements, individual backbone peptide resonances were selectively irradiated (with the decoupler) sufficiently long (0.05 to 0.5 s) to saturate the resonance. Then, following a 1-ms homogeneity-spoil pulse, the recovery of the equilibrium spin-state distribution was followed by observing the amide proton resonances after a variable delay time, τ, with a 2-1-4 tailored-pulse. As in the difference NOE measurements, the irradiation was turned off and its frequency temporarily switched to an off-resonance value during the homogeneity-spoil, spin-saturation recovery, and acquisition periods so as to avoid noise spikes at the frequency of amide proton irradiation. Fifty to five hundred free induction decays were summed and Fourier transformed for each spectrum. $T_{1,app}^{-1}$ was then obtained from the slope of a linear least-squares fit of $\ln \{[I(\infty) - I(\tau)]/I(\infty)\}$ plotted against τ.

Equation 1 is valid for backbone peptide protons provided that there are no other important relaxation processes, such as *cis/trans* isomerization of X-Pro peptide bonds or intermolecule solvent/solute relaxation processes, contributing to $T_{1,app}$. Since the characteristic time for *backbone* X-Pro peptide bond *cis/trans* isomerization in these peptides ($\sim$40 s at 27 °C, unpublished result) is much longer than the measured $T_{1,app}$, this process did not have to be taken into account. Similarly, intermolecular solvent/solute dipolar relaxation rates are assumed to be negligible[46,48,53] compared to those of intramolecular relaxation processes or proton exchange at the pH of these measurements (i.e., pH 6.0).

Measurement of Side-Chain Amide Proton Exchange Rates. For the primary amide protons of the Asn side chain, amide bond isomerization which interconverts protons *cis* and *trans* to the amide carbonyl (referred to here as CONH^1 and CONH^2, respectively) will contribute to the apparent T_1 relaxation. This effect must be taken into account in calculating k_{ex} and is done[53] by measuring both solvent/solute spin-saturation transfer for each side-chain amide proton, η_1 and η_2, as described above, and also *cis* $\rightarrow$ *trans* (η_{12}) and *trans* $\rightarrow$ *cis* (η_{21}) nuclear Overhauser enhancement and saturation transfer.

The values of η_{ji} and of $T_{1,app,i}$ for side-chain amide protons were determined simultaneously with the following experiment. Because the relaxation properties of the amide protons i and j are coupled (both by dipolar coupling and by slow side-chain *cis/trans* isomerization) both exhibit multiexponential spin-saturation recovery at 27 °C which is difficult to analyze experimentally. Krishna et al.[53] have pointed out that this problem can be overcome by following the saturation recovery of amide proton i while maintaining continuous saturation of amide proton j. In these measurements, both amide protons are saturated simultaneously by alternating 10-ms irradiation pulses between amide resonance frequencies ω_i and ω_j 100–200 times. The irradiation was then maintained at ω_j for a variable relaxation time during which amide proton i was allowed to relax. The irradiation at ω_j was then turned off and, following a 3-ms homogeneity-spoil and 10-ms homogeneity recovery period, the spectrum was obtained with a 2-1-4 tailored-pulse. The selectivity of the irradiating pulse at each of the two side-chain amide resonances was verified by the appropriate controls.

From these data, $T_{1,app,i}$ was then determined by the usual logarithmic plot. In addition, by comparing the intensities of resonances i and j after long (>10 s) delay times with their intensities in control spectra recorded with off-resonance irradiation, η_{ji} could also be determined. In summary, when $T_{1,app,i}$ and η_{ji} are determined by this double-irradiation method, the two experiments (irradiation of solvent, which gives η_i, and saturation recovery of spin i while maintaining continuous saturation of spin j, which gives $T_{1,app,i}$ and η_{ji}) provide three equations[53] which determine the three unknowns $T_{1,mag,i}$*, $k_{ex,i}$, and $k_{ij} - \sigma$, where $T_{1,mag,i}$* is the intrinsic longitudinal relaxation time of amide proton i, σ is a cross-term related to the NOE between sites i and j, and k_{ij} is the first-order rate constant for amide side-chain *cis/trans* (or *trans/cis*) isomerism. Simultaneous solution of these equations gives the pseudo-first-order rate constant for exchange of amide proton i, *viz.*

$$k_{ex,i} = (\eta_i - \eta_j\eta_{ji})/(T_{1,app,i}) \quad (2)$$

where

$$T_{1,app,i} = [T_{1,mag,i}^{-1} + k_{ij} + k_{ex,i}]^{-1} \quad (3)$$

and an expression for the intrinsic longitudinal relaxation time ($T_{1,mag,i}$*) shown in the next subsection.

Calculation of Peptide and Amide Intrinsic T_1 Relaxation Times. For backbone peptide protons, the intrinsic longitudinal proton relaxation time, $T_{1,mag}$, was determined by correcting the measured $T_{1,app}$ for the contribution to relaxation due to amide proton exchange:

$$T_{1,mag} = [T_{1,app}^{-1} - k_{ex}]^{-1} \quad (4)$$

For side-chain (i.e. primary amide) protons,[53] combination of eq 2 and 3 leads to:

$$T_{1,mag,i}^* = (T_{1,app,i})/(1 - \eta_i + \eta_j\eta_{ji}) \quad (5)$$

where

$$T_{1,mag,i}^* = [T_{1,mag,i}^{-1} + k_{ij}]^{-1} \quad (6)$$

when $T_{1,app}$ is measured by the double-irradiation method described above. Hence, for the side-chain amide protons, the reported intrinsic longitudinal relaxation times ($T_{1,mag,i}$*) retain a contribution from side-chain amide cis/trans isomerization.

NMR Sample Preparation. Owing to the acute pH sensitivity of amide proton exchange rates,[49,57,58] samples were prepared at 3–10 mg/mL in 5 mM phosphate buffer, in H_2O, at pH 6.00 ± 0.05. Ethylene diaminetetraacetic acid (0.1 mM) was included as a metal ion scavanger. The same buffer, which was saturated with N_2 to exclude paramagnetic O_2 prior to dissolving the peptides, was used for all measurements. In independent measurements, no measurable phosphate buffer catalysis of amide hydrogen exchange was observed, which is consistent with other reports.[57-60] A coaxial tube of D_2O was used for the spectrometer lock.

In NOE measurements, the sample pH was adjusted to 3.5, which corresponds approximately to the pH of slowest peptide proton exchange.[57,58]

Estimates of Error. The standard errors reported in $T_{1,app}$ measurements are standard errors of the slope of the $\ln \{[I(\infty) - I(\tau)]/I(\infty)\}$ vs. τ curve, unless otherwise noted. The intensities of non-exchangeable proton resonances (e.g., tyrosine ring protons) with and without solvent irradiation were always identical to within ±5%. Hence the standard error in the estimate of η was taken as ±0.07 $(1 - \eta)$, computed from the errors in measuring intensities, except where otherwise noted. This error includes any small solvent/solute NOE effects. In calculating k_{ex} and $T_{1,mag}$, error estimates were propagated in the usual manner.

Raman Spectroscopy. The instrument for recording Raman spectra at 22 °C has been described previously.[61] For the spectra of solutions, the 488.0-nm line of a Coherent CR3 argon ion laser at a power of 200–300 mW was focused on the sample. The spectra of crystalline Ac-Asn-Pro-Tyr-NHMe was also obtained with the 488.0-nm line, which was not focused, at a power of 40 mW. The instrumental resolution was <4 cm^{-1} for all spectra. Peak frequencies were calibrated with the 981-cm^{-1} symmetric stretching band of sulfate ion.

The range of concentrations in the Raman experiments was from 0.02 M (10 mg/mL) to 0.1 M (50 mg/mL); no concentration dependence of the Raman spectra was observed over this range. Amide vibrational modes were assigned on the basis of their characteristic sensitivity to deuterium exchange and by their frequencies.[62] To render all bands visible, difference spectra were obtained by subtracting the solvent (D_2O or H_2O) spectrum from the solution spectrum on the computer. Deuterated amide compounds were prepared by multiple cycles of lyophilization from D_2O.

X-ray Crystallography. Single crystals of synthetic Ac-Asn-Pro-Tyr-NHMe were obtained from H_2O (form I) and also as the ethanol solvate (form II) from acetone/hexanes/ethanol (1:1:2). Ac-Tyr-Pro-Asn-NHMe and Ac-Tyr-Pro-NHMe were both crystallized as the dihydrate, from DMF/H_2O (1:10) and H_2O, respectively. The three crystals which contained solvent grew in the shape of long, thin needles, while crystals of Ac-Asn-Pro-Tyr-NHMe obtained from H_2O had approximately cubic form. The essential data for all four crystals studied are summarized in Table I.

All single-crystal X-ray diffraction measurements were made with a computer-controlled Syntex $P2_1$ diffractometer. Preliminary X-ray photographs demonstrated that each of the four crystals belonged to the orthorhombic crystal system, and the pattern of systematic extinctions ($h00$: $h = 2n + 1$; $0k0$: $k = 2n + 1$; $00l$: $l = 2n + 1$) uniquely determined the space group as $P2_12_12_1$ for each crystal. The unit cell dimensions reported in Table I were determined in each case by a least-squares fitting of 15 diffractometer-measured reflections with moderate 2θ values ($25° < 2\theta < 40°$ for Cu Kα radiation).

(57) Molday, R. S.; Kallen, R. G. *J. Am. Chem. Soc.* **1972**, *94*, 6739.
(58) Molday, R. S.; Englander, S. W.; Kallen, R. G. *Biochemistry* **1972**, *11*, 150.
(59) Leichtling, B. H.; Klotz, I. M. *Biochemistry* **1966**, *5*, 4026.
(60) Englander, S. W.; Poulsen, A. *Biopolymers* **1969**, *7*, 379.
(61) Scheule, R. K.; Van Wart, H. E.; Vallee, B. L.; Scheraga, H. A. *Proc. Natl. Acad. Sci. U.S.A.* **1977**, *74*, 3273.
(62) Van Wart, H. E.; Scheraga, H. A. In "Methods in Enzymology, Enzyme Structure, Part G"; Hirs, C. H. W., Timasheff, S. N., Eds.; Academic Press, New York, 1978; Vol. 49, p 67.

Table I. Single-Crystal Data

	Ac-Asn-Pro-Tyr-NHMe		Ac-Tyr-Pro-Asn-NHMe	Ac-Tyr-Pro-NHMe
	crystal form I	crystal form II		
cryst solvent	H_2O	acetone/hexanes/ethanol 1:1:2	DMF/H_2O 1:10	H_2O
size of crystal, mm	0.4 × 0.3 × 0.3	0.7 × 0.1 × 0.1	0.6 × 0.06 × 0.05	0.6 × 0.1 × 0.08
space group	$P2_12_12_1$	$P2_12_12_1$	$P2_12_12_1$	$P2_12_12_1$
formula of asymmetric unit, FW	$C_{21}H_{29}N_5O_6$, 447.49	$C_{21}H_{29}N_5O_6 \cdot C_2H_5OH$, 493.56	$C_{21}H_{29}N_5O_6 \cdot 2(H_2O)$, 483.52	$C_{17}H_{23}N_3O_4 \cdot 2(H_2O)$, 369.42
unit cell dimensions (Å) ($\alpha = \beta = \gamma = 90.0°$)				
a	17.587 (2)	25.770 (3)	26.490 (6)	14.337 (2)
b	13.413 (2)	12.848 (2)	10.924 (3)	13.821 (2)
c	9.912 (1)	7.476 (2)	8.598 (2)	9.872 (2)
calcd density, g/cm^3	1.27	1.32	1.29	1.25
radiation used, λ, Å	Cu Kα, 1.54178	Mo Kα, 0.71069	Cu Kα	Cu Kα
no. of unique data obsd[a]/total (fraction observed)	1653/1816 (91.0%)	1291/2016 (64.0%)	1191/1949 (61.1%)	1078/1526 (70.6%)
R factors[b] for final X-ray model R_1/R_2	0.047/0.067	0.064/0.075	0.076/0.090	0.062/0.075

[a] $|F_{obsd}| > 3\sigma(F_{obsd})$. [b] $R_1 = \{\sum||F_o| - |F_c||\}/\sum|F_o|$. $R_2 = [\{\sum w(|F_o| - |F_c|)^2\}/\sum w|F_o|^2]^{1/2}$; $w = 1/\sigma^2(F_o)$. $\sigma(F_o) = [I_{scan} + \{I_{bgd}/(\text{bgd time/scan time})^2\}]^{1/2} + 0.03|F_o|$, where I_{scan} and I_{bgd} are the X-ray intensities in peak and background regions of the diffraction pattern, respectively, and scan and bgd times are the corresponding counting times.

Table II. Backbone Dihedral Angles for the Four Single Crystal Structures and for Some β-Bends at Relevant Sequences in Native Protein Structures

		Ac-Asn-Pro-Tyr-NHMe		His-Pro-Tyr[c] porcine elastase	ideal type I[d] β-bend			Ac-Tyr-Pro-Asn-NHMe[b]	Ac-Tyr-Pro-NHMe[b]	Tyr-Pro-Asn[e] concanavalin A
		form I[a]	form II[b]							
Asn	φ	−101	−108			Tyr	φ	−90	−71	
	ψ	106	108				ψ	156	149	
	ω	−175	−176				ω	163	−178	
Pro	φ	−58	−60	−62	−60	Pro	φ	−67	−75	−66
	ψ	−27	−28	−18	−30		ψ	141	144	127
	ω	−179	−172	179	180		ω	−173	−178	180
Tyr	φ	−80	−90	−93	−90	Asn	φ	−88		83
	ψ	−8	−5	−1	0		ψ	−19		−33
	ω	−175	−179	178	180		ω	−176		180

[a] Standard deviations 0.5–1.0°. [b] Standard deviations 1.0–2.0°. [c] Residues 91–93 in native porcine elastase (type I β-bend); ref 67. [d] Ideal bend geometries are defined in ref 30. [e] Residues 67–69 in concanavalin A (type II β-bend); ref 34.

With use of a variable-speed 1° ω-scan, an octant of data was collected out to a nominal resolution of 0.9 Å ($2\theta \leq 114°$ for Cu Kα radiation) for each of the four crystals reported. Although intensity data were collected with the crystals of Ac-Asn-Pro-Tyr-NHMe (form II) and Ac-Tyr-Pro-NHMe sealed in Lindemann capillaries and the crystal of Ac-Tyr-Pro-Asn-NHMe encased with epoxy, these three crystals which contained solvent were very thin needles and diffracted only weakly at higher scattering angles. Periodic monitoring of the intensities of three check reflections indicated that no serious decomposition of the crystals occurred during the collection of X-ray intensity data. No absorption corrections were made.

All four crystal structures were solved by multisolution direct methods.[63] The solutions to the phase problem were achieved by using five or more reflections with restricted phases in the starting set. The structures were refined by block-diagonal least squares using $1/\sigma^2(F_o)$ weighting.[63] The positions of hydrogen atoms were identified from different Fourier syntheses, where possible, and the remainder were calculated by using idealized bond geometry and an assumed C–H bond length of 1.02 Å (a compromise between values of ~1.10 and ~0.98 Å obtained from neutron[64] and X-ray diffraction[65] studies, respectively, of crystalline

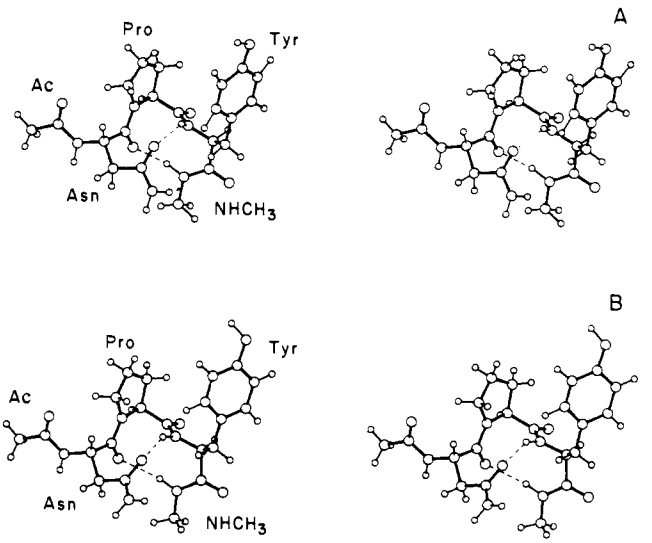

Figure 2. Stereoscopic representations of the crystal structures of Ac-Asn-Pro-Tyr-NHMe: (A) form I and (B) form II.

L-alanine). Both hydrogens of the asparagine side-chain amide were successfully located by difference Fourier synthesis in all three structures which contained asparagine; this provided an independent check on the distinction between the structurally similar *N*-acetyl group and the asparagine side chain for the two crystal forms of Ac-Asn-Pro-Tyr-NHMe. The tyrosine hydroxyl hydrogen atom was found by the difference

(63) All crystallographic calculations were carried out on a PRIME 850 computer, operated by the Cornell Chemistry Computing Facility. Principal programs employed were (a) REDUCE and UNIQUE data reduction programs, Leonowicz, M. E., Cornell University, 1978; (b) MULTAN78, "A system of Computer Programs for the Automatic Solution of Crystal Structures from X-ray Diffraction Data", Main, P., Hull, S. E., Lessinger, L., Germain, G., Declercq, J.-P., Woolfson, M. M., University of York, England, 1978; (c) NQEST, CYBER 173 version, negative quartets figure of merit calculation, Weeks, C. M., Medical Foundation of Buffalo, Inc., August 1976; (e) BLS78A, anisotropic block-diagonal least-squares refinement, Hirotsu, K., Arnold, E., Cornell University, 1980; (f) ORTEP; crystallographic illustration program: Johnson, C. K., Oak Ridge, ORNL-3794. For a summary description of MULTAN see: Germain, G.; Main, P.; Woolfson, M. M. *Acta Crystallogr., Sect. B* **1970**, *B26*, 274–285. Woolfson, M. M. *Acta Crystallogr., Sect. A* **1977**, *A33*, 219–225. For a summary of NQEST, refer to: De Titta, G. T.; Edmonds, J. W.; Langs, D. A.; Hauptman, H. *Acta Crystallogr., Sect. A* **1975**, *A31*, 472–479.

(64) Lehmann, M. S.; Koetzle, T. F.; Hamilton, W. C. *J. Am. Chem. Soc.* **1972**, *94*, 2657.

(65) Simpson, H. J., Jr.; Marsh, R. E. *Acta Crystallogr.* **1966**, *20*, 550.

Fourier technique in all structures except that of Ac-Tyr-Pro-NHMe. Block-diagonal least-squares refinements, with anisotropic non-hydrogen atoms and isotropic (fixed) hydrogen atoms, in each case converged to a model for which the standard unweighted crystallographic R factor was less than 0.076.

Results and Interpretations

Peptide Structures in the Solid State.[66] Figure 2, parts A and B, shows stereoscopic representations of the X-ray models of the two crystal forms of Ac-Asn-Pro-Tyr-NHMe. All peptide bonds in the two structures are *trans*. Table II gives a listing of the backbone dihedral angles for the four crystal structures and of the backbone dihedral angles for some β-bends at relevant sequences in native protein structures determined by X-ray crystallographic analysis.[34,67] Both forms I and II of Ac-Asn-Pro-Tyr-NHMe show a type I β-bend at the sequence Pro-Tyr, accompanied by a backbone/backbone hydrogen bond from the terminal NH-methyl amide hydrogen to the asparagine backbone carbonyl oxygen atom.

The presence of an additional backbone/side-chain intramolecular hydrogen bond from the tyrosine amide hydrogen to the asparagine side-chain carbonyl oxygen (Tyr-NH···O$^{\delta 1}$Asn) causes the structure to be even more compact. The relative distances of these two intramolecular hydrogen bonds are reversed in the two crystal forms of Ac-Asn-Pro-Tyr-NHMe (cf. Figure 2, A and B): the backbone methyl amide NH nitrogen to asparagine backbone carbonyl oxygen hydrogen bond distances are 2.91 and 3.28 Å, respectively, and the tyrosine NH nitrogen to asparagine side-chain carbonyl oxygen distances are 3.12 and 3.05 Å, respectively, for forms I and II. In addition, several intermolecular peptide–peptide and peptide–solvent hydrogen bonds were observed (see supplementary Table S-5).[66] In both crystal forms, the Tyr OH is an intermolecular hydrogen bond donor, the acceptor being the backbone tyrosine carbonyl oxygen in form I (oxygen/oxygen interatomic distance of 2.67 Å) and the backbone acetyl carbonyl oxgyen in form II (oxygen/oxygen interatomic distance of 2.68 Å).

Inspection of Table II shows that the backbone conformations of the Pro-Tyr portion of both crystal forms of this tripeptide model very closely approximate the type I β-bend found in the His^{91}-Pro^{92}-Tyr^{93} sequence of porcine elastase. Significantly, the bend conformation of His-Pro-Tyr in the crystal structure of porcine elastase[67] also involves backbone/backbone (Trp^{94}-NH···O-His^{91}, nitrogen/oxygen interatomic distance of 2.83 Å) and backbone/side-chain (Tyr^{93}-NH···N$^{\delta 1}$His^{91}, nitrogen/nitrogen interatomic distance of 3.16 Å) hydrogen bonds. A backbone/backbone hydrogen bond also stabilizes the type III β-bend in residues Asn^{67}-Pro^{68}-Tyr^{69} of bovine phospholipase A$_2$[35] (Thr^{70}-NH···O-Asn^{67}, nitrogen/oxygen interatomic distance of 2.87 Å). (It should be noted that type III and type I bends are similar.[68])

Although the two forms of Ac-Asn-Pro-Tyr-NHMe exhibit a reversal of intramolecular hydrogen bond lengths and different patterns of intermolecular hydrogen bonding in the crystal, the two conformations are very similar (cf. Figure 2, A and B). The largest difference between the conformations of Ac-Asn-Pro-Tyr-NHMe form I and form II is in the orientation of the terminus of the asparagine side chain:[69] viz. $\Delta\chi^1$(Asn) = 12.1° and $\Delta\chi^2$(Asn) = 31.8°. These differences may be due in part to the presence in form II of a hydrogen bond from an ethanol solvent molecule to the asparagine side-chain oxygen (EtOH···O$^{\delta 1}$Asn, with an oxygen/oxygen interatomic distance of 2.75 Å). Other significant differences between the two crystalline conformations

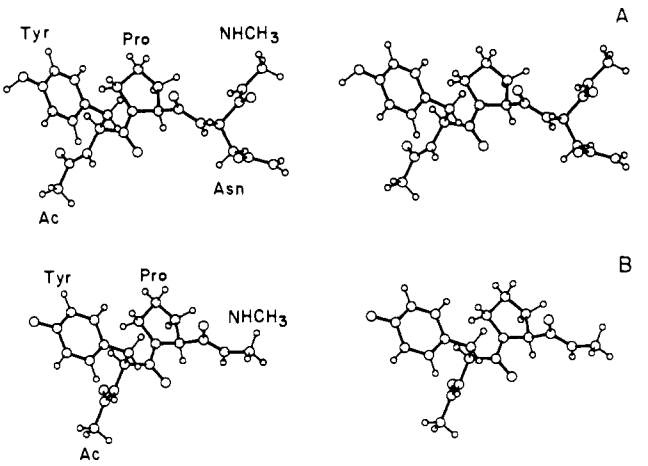

Figure 3. Stereoscopic representations of the crystal structures of (A) Ac-Tyr-Pro-Asn-NHMe and (B) Ac-Tyr-Pro-NHMe.

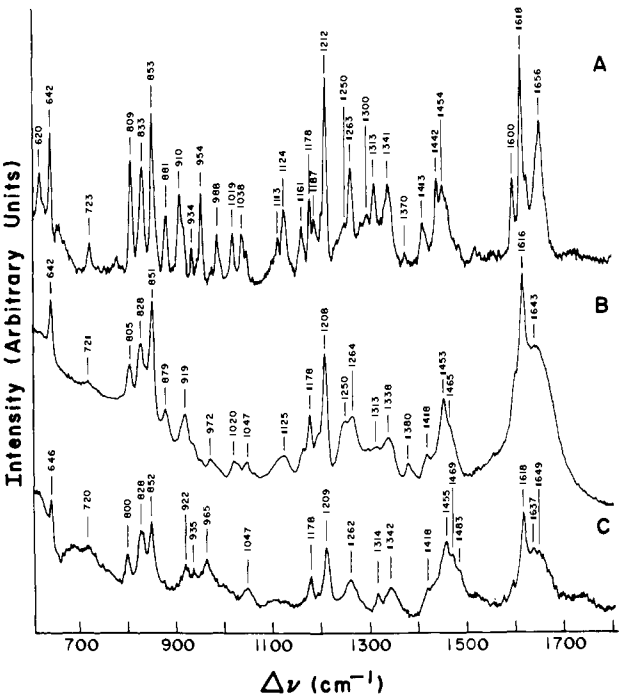

Figure 4. Raman spectra of Ac-Asn-Pro-Tyr-NHMe (A) crystallized from H_2O, (B) in H_2O, and (C) in D_2O. The peaks at 1250, ca. 1300, and 1380 cm^{-1} in the solution spectra in H_2O are assigned to amide III (predominantly N–H bending) modes on the basis of their characteristic frequency and sensitivity to deuteration (cf. parts B and C).

of Ac-Asn-Pro-Tyr-NHMe involve the orientation of the tyrosine ring [$\Delta\chi^1$(Tyr) = 10.4° and $\Delta\chi^2$(Tyr) = 10.7°] and the conformations of the pyrrolidine rings in the proline residues [$\Delta\chi^2$(Pro) = 15.0° and $\Delta\chi^3$ = 13.9°].

Figure 3, A and B, shows stereoscopic representations of X-ray models of Ac-Tyr-Pro-Asn-NHMe and Ac-Tyr-Pro-NHMe, respectively. Both of these structures have extended peptide backbone conformations, with all *trans*-peptide bonds, and no intramolecular hydrogen bonds. The backbone dihedral angle data for these two structures are also given in Table II along with data for a type II β-bend found in the Tyr^{67}-Pro^{68}-Asn^{69} sequence of concanavalin A.[34]

Peptide Conformations in Water. Previous studies[42] showed a doubling of resonances in the proton NMR spectra of these compounds, due to the presence of both *cis*- and *trans*-X-Pro conformations. In this paper, we concentrate on the major (*trans*) species. In the following paper,[22] we shall also examine the *cis* species.

NMR and Raman spectroscopoic data indicate that a significant fraction of the *trans*-Ac-Asn-Pro-Tyr-NHMe molecules

(66) The following solid-state data are available for each crystal structure in the form of supplementary tables. Table S-1: Fractional Coordinates and Thermal Parameters; Table S-2: Interatomic Bond Distances; Table S-3: Bond Angles; Table S-4: Torsional Angles; Table S-5: Distances for Hydrogen Bonds and Heteroatom contacts; Table S-6: Observed and Calculated Structure Factor Magnitudes and Calculated Phase Angles.

(67) Sawyer, L.; Shotton, D. M.; Watson, H. C. *Biochem. Biophys. Res. Commun.* **1973**, *53*, 944.

(68) Némethy, G.; Scheraga, H. A. *Biochem. Biophys. Res. Commun.* **1980**, *95*, 320.

(69) $\Delta\chi \equiv \chi^i_{\text{Form I}} - \chi^i_{\text{Form II}}$.

adopt hydrogen-bonded β-bend structures in water. The *trans*-Ac-Tyr-Pro-Asn-NHMe molecules also have a significant fraction of conformations in which the Asn-NHMe amide proton is hydrogen bonded.

1. Raman Spectroscopy. The Raman spectra for Ac-Asn-Pro-Tyr-NHMe in the crystalline form, in H_2O, and in D_2O are presented in Figure 4. In going from the crystal phase to H_2O solution, all the vibrational modes of Ac-Asn-Pro-Tyr-NHMe are broadened, a manifestation both of the variety of solvent environments which exist and the distribution of molecular conformations which are accessible in water. Of particular interest in these spectra is the 1380-cm^{-1} amide III (or predominantly N–H bending) mode of Ac-Asn-Pro-Tyr-NHMe in H_2O (Figure 4B), which is assigned on the basis of its frequency and sensitivity to deuteration. This mode is also observed in the Raman spectra (not shown here) in H_2O of Ac-Ala-Pro-Tyr-NHMe and Ac-Asn-Pro-NHMe but not in Ac-Pro-Tyr-NHMe.

While amide III (or predominantly N–H bending) modes of peptides generally range[62,70] from 1210 to 1320 cm^{-1}, deuterium-sensitive Raman modes in the 1300–1400 cm^{-1} region are often associated with hydrogen-bonded β-bend conformations.[71-74] Normal mode calculations on idealized β-bend conformations[71] and on energy-minimized β-bend conformations of cyclic peptides[73,74] predict N–H bending modes with frequencies ranging from 1290 to 1330 and 1230 to 1430 cm^{-1}, respectively. Raman spectra of *cyclo*(L-Ala-Gly-Aca)[73] and *cyclo*(L-Ala-D-Ala-Aca),[74] both of which are model type II β-bends, and of *cyclo*(L-Ala-L-Ala-Aca),[74] which is a model type I (or III) β-bend, also exhibit deuterium-sensitive modes at 1375–1380 cm^{-1} both in H_2O and in the solid state. By analogy with these studies, the ~1380-cm^{-1} N–H bending mode of Ac-Asn-Pro-Tyr-NHMe is tentatively attributed to a significant population of hydrogen-bonded β-bend conformers with *trans*-Asn-Pro peptide bonds in H_2O. We cannot, however, rule out the possibility that the deuterium-sensitive ~1380-cm^{-1} band is due to nonbend intramolecularly hydrogen bonded structures.

In addition to the deuterium-sensitive 1380-cm^{-1} band of the Raman spectrum in water, bands at 1250 and ca. 1300 cm^{-1} are also affected by deuteration (cf. Figure 4, parts B and C) and, thus, are assigned to amide III modes. Modes of similar frequency were also observed in crystalline Ac-Asn-Pro-Tyr-NHMe (Figure 4A). Since N–H bending modes are generally very sensitive to variation in backbone dihedral angles,[75] the presence of amide III or N–H bending modes of similar frequency in the crystal and in aqueous solutions (i.e at 1250 and 1300 cm^{-1}) indicate that the type I β-bend conformation present in the solid state has backbone conformational features similar to those of the dominant solution conformation. On the other hand, although a weak band at ~1370 cm^{-1} is observed in the solid-state Raman spectrum, the characteristic 1380-cm^{-1} band of the solution spectrum is not present. Hence, the solution backbone conformation must differ (to some extent) from that of the solid state.

The strong doublet at ~850 and ~830 cm^{-1} in the Raman spectra of Tyr-containing polypeptides has been assigned[76] to Fermi resonance between a ring-breathing vibration and the overtone of an out-of-plane ring-bending mode of para-substituted benzenes. Empirically, the intensity ratio of this doublet has been correlated with the hydrogen-bonding environment and state of ionization of the phenolic hydroxyl group. For the synthetic peptides, the 850:830 intensity ratios are 0.91 for L-Tyr (H_2O), 1.20 for Ac-Pro-Tyr-NHMe (H_2O), 1.28 for Ac-Ala-Pro-Tyr-NHMe (H_2O), 1.50 for Ac-Asn-Pro-Tyr-NHMe (H_2O), and 1.55 for Ac-Asn-Pro-Tyr-NHMe (crystal form I). The significance of these data is addressed in the Discussion section.

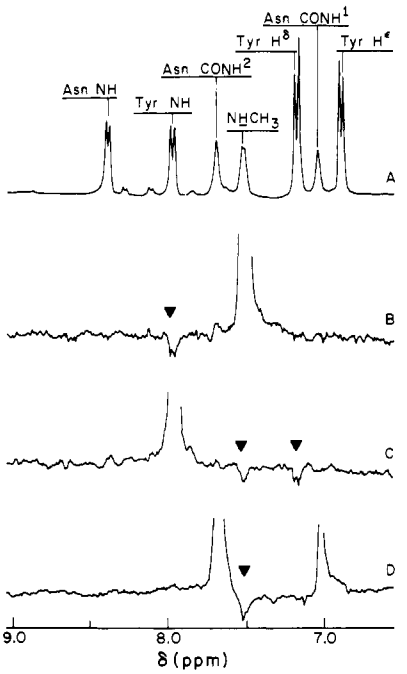

Figure 5. NOE measurements for amide protons of Ac-Asn-Pro-Tyr-NHMe in H_2O. (A) Assignments of amide and aromatic protons. The upfield Asn side-chain amide proton is designated Asn-CONH^1 and is assigned (see text) to the amide proton *cis* to the side-chain carbonyl oxygen. The downfield Asn side-chain amide proton is designated Asn-CONH^2 and is assigned (see text) to the amide proton *trans* to the side-chain carbonyl oxygen. The minor resonances have been assigned[42] to the ensemble of conformations with *cis*-Asn-Pro peptide bonds. (B) Difference NOE, with irradiation of the NHMe resonance compared with irradiation 5000-Hz upfield. (C) Difference NOE spectrum, with irradiation of the Tyr NH compared with irradiation 5000-Hz upfield. (D) Difference NOE spectrum, with irradiation at the Asn-CONH^2 resonance compared with irradiation 100-Hz upfield (see Experimental Section). This symmetric irradiation technique controls for the nonselectivity of the irradiation pulse, which results in a small negative peak at the Tyr-H$^\delta$ resonance frequency. The small amount of nonselective irradiation of the Tyr-H$^\delta$ resonance demonstrates the selectivity of the irradiation pulse used. The concentration of all samples was 10 mg/mL at pH 3.5 and 27 °C.

Because of its lower solubility in water, Raman spectroscopic measurements which require concentrations ≥10 mg/mL have not been made on solutions of Ac-Tyr-Pro-Asn-NHMe.

2. Proton/Proton NOE Measurements in H_2O. Supporting evidence for a β-bend conformation of *trans*-Ac-Asn-Pro-Tyr-NHMe in H_2O is obtained from difference NOE measurements (Figure 5). NOE's indicating short (≲3 Å) through-space interproton distances in at least some fraction of the molecules with *trans*-Asn-Pro peptide bonds were observed for NHCH$_3$ → Tyr NH (+3.3%, Figure 5B), Tyr NH → NHCH$_3$ (+2.3%, Figure 5C), Tyr NH → Tyr H^δ (+2.5%, Figure 5C) and Asn CONH^2 → NHCH$_3$ (+2.9%, Figure 5D). These NOE's are consistent with a β-bend conformation (see Discussion section).

The positive peak at ~7.0 ppm in the NOE difference spectrum of Figure 5D represents *trans* → *cis* saturation transfer (and NOE) for Asn CONH^2 to Asn-CONH^1, due to *trans*/*cis* isomerization about the *side-chain* amide bond. No saturation transfer due to *trans*/*cis* isomerization about the *backbone* peptide bond is observed at this temperature.

These NOE's, measured at pH 3.5 (which is near the minimum of the acid/base catalyzed amide proton exchange curve[57,58]), were not observed at higher pH where the contribution of exchange to proton relaxation quenches the NOE. Even at pH 3.5, proton exchange probably quenches the observable NOE to some extent.

(70) Peticolas, W. L.; Cutrera, T.; Rodgers, G. R. In "Biomolecular Structure, Conformation, Function and Evolution"; Srinivasan, R., Ed.; Pergamon Press: Oxford, 1981; p 45.
(71) Krimm, S.; Bandekar, J. *Biopolymers* **1980**, *19*, 1.
(72) Bandekar, J.; Krimm, S. *Biopolymers* **1980**, *19*, 31.
(73) Maxfield, F. R.; Bandekar, J.; Krimm, S.; Evans, D. J.; Leach, S. J.; Némethy, G.; Scheraga, H. A. *Macromolecules* **1981**, *14*, 997.
(74) Bandekar, J.; Evans, D. J.; Krimm, S.; Leach, S. J.; Lee, S.; McQuie, J. R.; Minasian, E.; Némethy, G.; Pottle, M. S.; Scheraga, H. A.; Stimson, E. R.; Woody, R. W. *Int. J. Peptide Protein Res.* **1982**, *19*, 187.
(75) Hsu, S. L.; Moore, W. H.; Krimm, S. *Biopolymers* **1976**, *15*, 1513.
(76) Siamwiza, M. N.; Lord, R. C.; Chen, M. C.; Takamatsu, T.; Harada, I.; Matsuura, H.; Shimanouchi, T. *Biochemistry* **1975**, *14*, 4870.

Table III. Solvent Saturation Transfer and Longitudinal Relaxation Data for Terminally Blocked Amino Acids and Peptides[a] at pH 6.00 ± 0.05, 27 °C

proton resonance[b]	Asn		Tyr		Pro-Tyr		Asn-Pro-Tyr		Tyr-Pro-Asn	
	η[c]	$T_{1,app}$,[d] s	η	$T_{1,app}$, s	η	$T_{1,app}$, s	η	$T_{1,app}$, s	η	$T_{1,app}$, s
Asn-N*H*	0.89 ± 0.01[e]	0.19 ± 0.01[e]					0.78 ± 0.05[e]	0.12 ± 0.01	0.80 ± 0.02	0.12 ± 0.01[e]
Asn-CON*H*^{1}	0.60 ± 0.01	0.18 ± 0.01					0.29 ± 0.05[e]	0.29 ± 0.01	0.44 ± 0.04	*f*
Asn-CON*H*^{2}	0.66 ± 0.02	0.13 ± 0.01					0.36 ± 0.03[e]	0.13 ± 0.01	0.50 ± 0.04	*f*
Tyr-N*H*			0.54 ± 0.03	0.72 ± 0.01	0.53 ± 0.03	0.34 ± 0.03	0.28 ± 0.03[e]	0.38 ± 0.04[e]	0.47 ± 0.04	0.41 ± 0.03[e]
N*H*-CH_3	0.62 ± 0.01[e]	0.76 ± 0.09[e]	0.47 ± 0.04	0.86 ± 0.01	0.47 ± 0.04	0.66 ± 0.05	0.21 ± 0.07[e]	0.66 ± 0.05[e]	0.39 ± 0.04	0.58 ± 0.03[e]

[a] *N*-Acetyl-*N'*-methylamides. In proline containing peptides, values are reported only for the ensemble of conformations with *trans*-X-Pro peptide bonds. [b] The upfield Asn side-chain amide proton is designated Asn-CON*H*^{1}, while the downfield Asn side-chain amide proton is designated CON*H*^{2}. [c] η is the fractional decrease in amide proton intensity due to steady-state saturation of the H_2O resonance. [d] $T_{1,app}$ is the apparent longitudinal relaxation time uncorrected for contribution of proton exchange. For Asn side-chain amide protons *i* and *j*, $T_{1,app}$ for resonance *i* is measured while resonance *j* is continuously maintained saturated. [e] These error estimates represent the ranges of values obtained in multiple independent measurements. [f] Values could not be determined accurately because partial overlap of Asn CON*H*^{1} with Tyr H$^{\epsilon}$ resonance complicates T_1 measurement at 27 °C.

The tendency of Ac-Tyr-Pro-Asn-NHMe to crystallize at concentrations approaching 10 mg/mL precludes its study by NOE measurements in H_2O.

3. Identification of Backbone Amide Hydrogen Bonds. In order to obtain direct evidence for intramolecular hydrogen bonds in H_2O which are often associated with β-bend conformations, we have used the method of solvent spin-saturation transfer[46-56] to measure the pseudo-first-order rate constants for amide proton exchange in both *trans*-Ac-Asn-Pro-Tyr-NHMe and *trans*-Ac-Tyr-Pro-Asn-NHMe. The interpretation of these measurements was made by comparing these exchange rates with those of the corresponding *N*-acetyl-*N'*-methyl amino acid amides and of Ac-Pro-Tyr-NHMe measured under the same conditions and by the same technique.

In interpreting these results, it is necessary to account for primary sequence effects on amide proton exchange rates, which are well understood for backbone (i.e., secondary) amide protons[57,58,77] and appear to follow some simple rules. At pH greater than ~5, the rate of backbone amide proton exchange is determined predominantly by specific hydroxide catalysis. Since base-catalyzed exchange involves direct deprotonation of the amide NH,[78] electron-withdrawing substituents which make the amide a stronger acid are generally observed to enhance base-catalyzed exchange. At the pH of our amide proton exchange measurements (6.0 ± 0.05), replacement of a terminal blocking group with a (terminally blocked) amino acid should, in the absence of conformational effects, result in an *increased* (or unaffected) pseudo-first-order rate constant for amide exchange because of the increased (or unaffected) negative inductive effect on nearest-neighbor peptides. In addition to this backbone primary sequence effect, neighboring amino acid side chains influence secondary amide exchange rates by inductive and charge effects,[58,77] so that comparisons of rate constants are meaningful only between peptide bond amides involving the same amino acid pair (or blocking group).

Only *nearest-neighbor* peptide bonds and side chains[58] play a significant role in primarily inductive primary sequence effects arising from backbones and side chains, respectively. In light of these facts, we anticipate that, in considering the amide proton of a particular peptide bond, extension of the polypeptide chain by replacement of terminal blocking groups with (terminally blocked) amino acids will result in higher pseudo-first-order proton exchange rate constants (at pH 6) or have no measurable effect on the exchange rate unless conformational features (e.g., intramolecular hydrogen bonds) retard proton exchange in some fraction of the molecules.

The fractional decrease in amide proton resonance intensities (η) due to steady-state saturation of the H_2O solvent spin-states and apparent longitudinal relaxation times ($T_{1,app}$) for the backbone and side-chain amide protons in these molecules are presented in Table III. All saturation recovery curves were monoexponential (when side-chain amides were meausred by the method described in the Experimental Section) with linear correlation coefficients

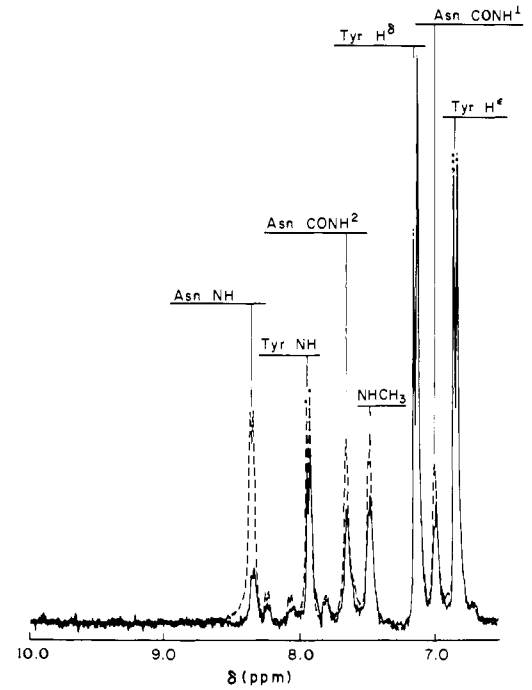

Figure 6. Solvent spin-saturation transfer measurement on Ac-Asn-Pro-Tyr-NHMe. Spectra were recorded either without (---) or with steady-state saturation of the H_2O resonance (—). Sample concentration was 5 mg/mL at pH 6.0 ± 0.05 and 27 °C.

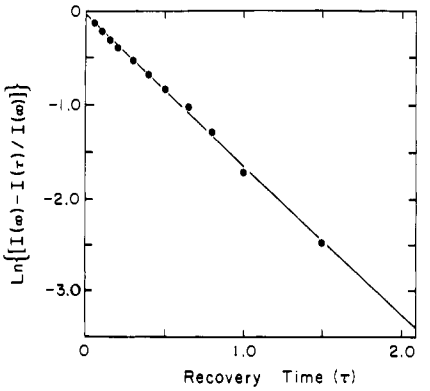

Figure 7. Amide proton spin-saturation recovery. The methyl amide proton of Ac-Asn-Pro-Tyr-NHMe, which is hydrogen bonded in ~50% of the molecules with *trans*-Asn-Pro peptide bonds, is shown as an example. The monoexponential behavior verifies that hydrogen-bonded conformations involving this proton have lifetimes which are short relative to the relaxation-time time scale.

$r > 0.99$, indicating that the rate constants calculated from these measurements represent time-averaged values for the ensemble of conformations with *trans*-X-Pro peptide bonds which interconvert (within the ensemble) at a rate which is fast relative to

(77) Englander, S. W.; Downer, N. W.; Teitelbaum, H. *Annu. Rev. Biochem.* **1972**, *41*, 903.

$T_{1,app}^{-1}$. Examples of a solvent spin-saturation transfer measurement (for all of the backbone and side-chain amide protons of Ac-Asn-Pro-Tyr-NHMe) and an amide proton saturation recovery measurement (for the N*H*Me proton of Ac-Asn-Pro-Tyr-NHMe) are presented in Figures 6 and 7, respectively.

The amide protons of all the compounds studied showed solvent spin-saturation transfer effects, with $0 < \eta < 1$, at pH 6.00 ± 0.05 and 27 °C, making these optimal conditions for comparing proton exchange rates. There is no evidence for a hydrogen-bonded tyrosine hydroxyl proton when using the Redfield tailored-pulse in either Ac-Asn-Pro-Tyr-NHMe ($\delta \sim 8$–10 ppm; see Figure 6) or Ac-Tyr-Pro-Asn-NHMe under these conditions.

Comparing the values of η measured for backbone amide protons (Table III), significantly lower amounts of solvent saturation-transfer were observed to the Tyr N*H* and N*H*-Me amide protons of Ac-Asn-Pro-Tyr-NHMe than for the corresponding protons of Ac-Pro-Tyr-NHMe and Ac-Tyr-NHMe, suggesting lower solvent accessibility of these protons in *trans*-Ac-Asn-Pro-Tyr-NHMe. The saturation transfer, however, depends on both the amide proton exchange rate constant and intrinsic longitudinal relaxation time, and therefore it cannot be correlated directly with structural features without explicitly calculating these two relaxation parameters.

The pseudo-first-order proton exchange rate constants (k_{ex}) and intrinsic magnetic longitudinal relaxation times ($T_{1,mag}$), calculated from the data of Table III, are presented for each peptide-bond type in Table IV. The anticipated enhancement of k_{ex} due to the primary sequence effect of adding peptide groups is clearly seen in several of the backbone amide protons including those of Ac-Asn (cf. Ac-Asn-NHMe and Ac-Asn-Pro-Tyr-NHMe in Table IV), Ac-Tyr (cf. Ac-Tyr-NHMe and Ac-Tyr-Pro-Asn-NHMe), and Tyr-N*H*Me (cf. Ac-Tyr-NHMe and Ac-Pro-Tyr-NHMe). k_{ex} for the Tyr-N*H*Me amide proton of Ac-Asn-Pro-Tyr-NHMe, however, is significantly smaller than that of either Ac-Pro-Tyr-NHMe or Ac-Tyr-NHMe, indicating the presence of conformational features that retard exchange in the terminally blocked tripeptide. Similarly, k_{ex} for the Pro-Tyr amide proton of Ac-Asn-Pro-Tyr-NHMe is much smaller than that of the corresponding proton of Ac-Pro-Tyr-NHMe. The data indicate restricted solvent accessibility of the Pro-Tyr and Tyr-N*H*Me backbone amide protons which we interpret as evidence for intramolecular hydrogen bonds in a significant fraction of the *trans*-Ac-Asn-Pro-Tyr-NHMe molecules.

The identification of these two hydrogen bonds in Ac-Asn-Pro-Tyr-NHMe is supported by the small values of $T_{1,mag}$ observed in all of its amide protons (Table IV) suggesting a population of *trans* molecules with compact structure. Furthermore, as we have pointed out elsewhere,[42] the Tyr NH and NHMe amide proton chemical shifts of *trans*-Ac-Asn-Pro-Tyr-NHMe are upfield from the corresponding protons of Ac-Pro-Tyr-NHMe and Ac-Tyr-NHMe, suggesting involvement of these amide protons of *trans*-Ac-Asn-Pro-Tyr-NHMe in intramolecular hydrogen bonds. Hydrogen bonds involving these same two amide protons were also identified by examining the temperature dependence of the amide proton chemical shifts in Me_2SO–d_6 (unpublished results).

The fraction of backbone hydrogen bonds at these two sites can be estimated under three assumptions; (i) that the amide proton exchange rate constant for an intramolecularly hydrogen-bonded amide proton is much smaller than that of an H_2O solvated amide proton, (ii) that inductive effects of non-nearest-neighbor peptide bonds and side chains on the amide exchange rate constants are negligible,[58] and (iii) that no intramolecular hydrogen bonds exist in Ac-Pro-Tyr-NHMe. With these assumptions, the fractions of *trans*-Ac-Asn-Pro-Tyr-NHMe molecules with Pro-Tyr and Tyr-N*H*Me hydrogen bonds, estimated[79] by comparing k_{ex} of this terminally blocked tripeptide with that of Ac-Pro-Tyr-NHMe, are 53% and 56%, respectively, at 27 °C. It should be noted that

Table IV. Calculated Pseudo-First-Order Amide Proton Exchange Rate Constants and Magnetic Longitudinal Relaxation Times for Terminally Blocked Amino Acids and Peptides[a] at pH 6.00 ± 0.05, 27 °C

	backbone peptide NH proton[b]										side-chain amide protons[c,d]			
	Ac-Asn		Ac-Tyr		Pro-Tyr		Pro-Asn		Asn-NHMe		Tyr-NHMe		Asn CONH[1]		Asn CONH[2]	
peptide	k_{ex}	$T_{1,mag}$	k_{ex}	$T_{1,mag}$	k_{ex}	$T_{1,mag}$	k_{ex}	$T_{1,max}$	k_{ex}	$T_{1,mag}$	k_{ex}	$T_{1,mag}$	k_{ex}	$T_{1,mag}$*	k_{ex}	$T_{1,mag}$*
Ac-Asn-NHMe	4.67 ± 0.27[e]	1.65 ± 0.17[e]							0.83 ± 0.09[e]	2.00 ± 0.24[e]			0.33 ± 0.09	0.41 ± 0.02	1.42 ± 0.18	0.39 ± 0.03
Ac-Tyr-NHMe			0.75 ± 0.04	1.56 ± 0.11							0.55 ± 0.05	1.62 ± 0.13				
Ac-Pro-Tyr-NHMe					1.56 ± 0.16	0.72 ± 0.07					0.72 ± 0.08	1.24 ± 0.13				
Ac-Asn-Pro-Tyr-NHMe	6.72 ± 0.52[e]	0.53 ± 0.12[e]			0.74 ± 0.11[e]	0.51 ± 0.06[e]					0.32 ± 0.10[e]	0.84 ± 0.10[e]	0.44 ± 0.22	0.33 ± 0.02	1.94 ± 0.37	0.17 ± 0.02
Ac-Tyr-Pro-Asn-NHMe			1.15 ± 0.13[e]	0.77 ± 0.08[e]			6.56 ± 0.61[e]	0.61 ± 0.08[e]	0.67 ± 0.07[e]	0.95 ± 0.08[e]						

[a] In proline-containing peptides, values are reported only for the ensemble of conformations with *trans*-X-Pro peptide bonds. [b] k_{ex} is given by eq 1 is in by eq 4. k_{ex} is in s^{-1} and $T_{1,mag}$ is in s. [c] The upfield Asn side-chain amide proton is designated Asn CONH[1], while the downfield Asn side-chain amide proton is designated Asn CONH[2]. [d] $k_{ex,1}$ and $k_{ex,2}$ are given by eq 2 and $T_{1,mag}$* by eq 5. [e] These error estimates represent the ranges of values obtained in multiple independent measurements.

(78) Berger, A.; Loewenstein, A.; Meiboom, S. *J. Am. Chem. Soc.* **1959**, *81*, 62.

(79) With these assumptions, $\alpha = 1 - [(k_{ex})_{NPY}/(k_{ex})_{PY}]$ is the fraction of molecules with a hydrogen bond.

Table V. Asparagine Side-Chain Primary Amide Intramolecular Saturation Transfer Measurements[a]

peptide[b]	η_{12}[c]	η_{21}[c]
Asn	0.51 ± 0.05	0.73 ± 0.04
Tyr-Pro-Asn	0.41 ± 0.10	*d*
Asn-Pro-Tyr	0.37 ± 0.09	0.45 ± 0.10

[a] Measurements made in 5 mM phosphate buffer, 0.1 mM EDTA, pH 6.00 ± 0.05, in H_2O at 27 ± 1 °C. Peptide concentration, 4–5 mg/mL. [b] *N*-acetyl-*N'*-methylamides. [c] η_{12} is the fractional decrease in the resonance of the amide proton *trans* to the side-chain carbonyl oxygen with steady-state saturation of the *cis* proton resonances. η_{21} is the corresponding parameter for the *cis* proton resonance. [d] Measurement complicated by partial overlap of Asn CONH^1 with Tyr H$^\epsilon$ resonance.

this large fraction of intramolecular hydrogen-bonded conformers cannot be attributed to intermolecular interactions since cryoscopic freezing-point depression measurements in H_2O demonstrate that this molecule is largely monomeric at the concentrations of these NMR measurements (see Experimental Section).

Comparison of the values of k_{ex} of the Asn-NHMe amide proton of Ac-Asn-NHMe and Ac-Tyr-Pro-Asn-NHMe (Table IV) also indicates a small population of *trans*-Ac-Tyr-Pro-Asn-NHMe molecules with a hydrogen bond. A hydrogen bond involving the amide proton was also identified by measurements of the temperature dependence of its chemical shift in Me_2SO-d_6 (unpublished result).

4. Side-Chain Amide Proton Exchange Rates. The upfield (CONH^1) and downfield (CONH^2) side-chain amide protons of Ac-Asn-NHMe were assigned by time-dependent difference truncated driven NOE measurements[80] in Me_2SO-d_6. Selective irradiation of the upfield Asn C$^\beta$H resonance results in a larger initial and steady-state NOE to the downfield (CONH^2) side-chain amide resonance than to the upfield (CONH^1) resonance, indicating that the former is *trans* with respect to the carbonyl oxygen. Similar assignments for primary amide protons have been made elsewhere.[49,53] The assignments of the corresponding side-chain amide resonances for Ac-Asn-NHMe, *trans*-Ac-Asn-Pro-Tyr-NHMe, and *trans*-Ac-Tyr-Pro-Asn-NHMe in water are made by analogy with this result.

In order to calculate k_{ex} properly for primary (e.g., side-chain) amide protons,[53] η_{12}, the fractional decrease in the intensity of amide proton resonance Asn CONH^2 (*trans* to the carbonyl oxygen) observed in steady state saturation of Asn CONH^1 (*cis* to the carbonyl oxygen) and the corresponding parameter η_{21} were also measured. These data are presented in Table V. The calculated values of k_{ex} and $T_{1,mag}$*, based on the data of Tables III and V, are presented in Table IV.

In base-catalyzed proton exchange, primary amide protons *trans* to the carbonyl oxygen exchange faster than *cis* amide protons,[49,53] as can be seen by comparing k_{ex} of Asn-CONH^1 and Asn-CONH^2 in Table IV. Although the value of k_{ex} for both side-chain amides is somewhat higher for *trans*-Ac-Asn-Pro-Tyr-NHMe than for Ac-Asn-NHMe, this effect is not sufficiently large to distinguish these rate constants within the estimated error of the measurements. The value of $T_{1,mag}$* of Asn CONH^2 of *trans*-Ac-Asn-Pro-Tyr-NHMe, however, is significantly lower than that measured for any of the other side-chain amide protons (see Table IV), which is supportive of the NOE measurements (see above), indicating that this proton is in the vicinity of the NHCH$_3$ group in at least a fraction of the molecules.

Discussion

Nucleation and Chain-Folding Initiation Structures. Before considering the significance of these results, it is first necessary to discuss some general features of the protein folding problem. Nucleation refers to the initiation of the transformation from an unstable to a more stable state (or conformation). In processes which are well described by a two-state mechanism, such as in homogeneous crystallization of supersaturated solutions or in phase transitions, nucleation corresponds to the rate-limiting step, after which further growth is energetically favorable. The corresponding "nucleation structure" is intrinsically unstable, representing a local free energy maximum which is a balance between positive surface and negative bulk free energy contributions.[81]

In multistate mechanisms (e.g., protein folding mechanisms which involve partially or incorrectly folded intermediates), analogies to the physics of phase transitions may be misleading and have led to confusion in the meaning of the term "nucleation". (For a discussion of this problem, see ref 82.) When folding intermediates exist, a nucleation process can be described for each intermediate, while the intermediates themselves may act as "nuclei" for subsequent folding events.

In order to avoid this semantic confusion, we have adopted the term *chain-folding initiation structure* to describe thermodynamically metastable local conformations which form rapidly along the polypeptide chain in the initial stages of folding. These local structures limit the conformational space accessible to the protein by specific short- and medium-range interactions thereby directing subsequent folding events and provide stabilized structures onto which the other parts of the polypeptide chain can fold. Early-forming folding intermediates may be regarded as *initiated* polypeptide chains containing one or more chain-folding initiation structures.

Characterizing Chain-Folding Initiation Structures. Chain-folding initiation structures are stabilized by local interactions which, presumably, have been evolutionally selected so as to fold the protein efficiently *under folding conditions*. For this reason, we propose that local structures defined by short- and medium-range interactions under conditions of temperature and solution composition for which the native protein is stable play an important role in the folding mechanism. This is the concept embodied in the folding mechanism of Tanaka and Scheraga.[6,7] Unfortunately, the cooperativity of most folding processes, attributable primarily to long-range interactions, makes it difficult to isolate partially folded intermediates under folding conditions in sufficient quantities or for sufficiently long periods of time to allow conformational analysis. One approach to this problem has been to concentrate on equilibrium local structures present in thermally unfolded proteins or in denaturing solvent systems. Local structures which are most stable under these conditions, however, do not necessarily correspond to structural intermediates present on folding pathways at ambient temperatures and at neutral pH.

Another approach to studying the local conformations which are favored under folding conditions is to study peptide fragments as models of the chain conformations which are accessible in the *initial stage*[6,7] of folding. The model peptides used in this study provide a system in which short-range interactions are divorced from long-range interactions, but they may lack some medium-range interactions which are also important in the initial stage of folding. We do not believe that Asn^{113}-Pro^{114}-Tyr^{115} or Tyr^{92}-Pro^{93}-Asn^{94} are themselves complete chain-folding initiation sites (we anticipate that the sizes of chain-folding initiation sites are probably larger than three residues). Rather, we suggest that local conformations (e.g., β-bends) present in these synthetic, terminally blocked fragments of ribonuclease will be incorporated into (larger) chain-folding initiation structures, and hence into the folding intermediates which they generate. It is for this reason that we have examined the two tripeptides Ac-Asn-Pro-Tyr-NHMe and Ac-Tyr-Pro-Asn-NHMe in this series of papers.

Conformational Analysis of Ac-Asn-Pro-Try-NHMe. In the solid state, the two structures of Ac-Asn-Pro-Tyr-NHMe (representing the most easily crystallized conformations present in two different aqueous solvents) are both type I β-bends, with *trans*-Asn-Pro peptide bonds and intramolecular hydrogen bonds involving the Tyr NH and NHMe amide protons. Spectroscopic measurements indicate that a similar structure also corresponds to the dominant conformation in aqueous solution at 27 °C.

(80) Wagner, G.; Wüthrich, K. *J. Magn. Reson.* **1979**, *33*, 675.

(81) Frenkel, J. "Kinetic Theory of Liquids"; Oxford University Press: London, 1946.

(82) Kim, P. S.; Baldwin, R. L. *Annu. Rev. Biochem.* **1982**, *51*, 459.

In water, Ac-Asn-Pro-Tyr-NHMe exists as an ensemble of conformations, ~12% of which have *cis*-Asn-Pro peptide bonds.[42] Several other minor conformations, with lifetimes ≳0.1 s, are also detected by the Tyr ring resonance pattern (unpublished results). The major *trans* population is an equilibrium mixture of intramolecular and solvent hydrogen-bonded species which interconvert rapidly on the relaxation-time and proton chemical-shift time scales, having lifetimes less than about 1 ms. Intramolecular hydrogen bonds involving the Tyr NH or NHMe amide protons, like those in the crystal structure, are present in ~50% of the molecules with *trans*-Asn-Pro peptide bonds.

The Asn CONH^2/NHMe NOE in water provides strong additional evidence for a population of β-bend conformations of *trans*-Ac-Asn-Pro-Tyr-NHMe. This NOE provides a distance constraint which severely limits the conformational space accessible to a *trans* conformer and is consistent with (although apparently shorter than) the Asn CONH^2/NHMe interproton distance in the crystal structure of form I (crystallized from H_2O), viz. 4.03 Å. The observation of the Asn CONH^2/NHMe NOE in solution suggests that the Asn side-chain carbonyl oxygen is the acceptor of the TyrNH and/or NHMe hydrogen bond donor(s).

The Tyr NH/NHCH$_3$ NOE also provides supportive evidence for a population of β-bend conformers. The observation of this NOE in H_2O (with presumably some quenching due to proton exchange) suggests that it is relatively strong. On the basis of NOE measurements on similar small rigid molecules, we assume an upper limit of ~3 Å for this interproton distance. This conformational constraint[83] requires $|\psi_{Tyr}| < 90°$, for any value of ϕ_{Tyr}, and is consistent with the observed values in the crystal structures of forms I and II, respectively, of *trans*-Ac-Asn-Pro-Tyr-NHMe ($\psi_{Tyr} = -8°$ and $-5°$) in which the type I β-bend is adopted. The Tyr NH → Tyr H^δ NOE, which is also observed, arises strictly from the geometric constraints of the amino acid residue structure and cannot be used for conformational information.

Model building indicates that the acceptor of the *N*-methylamide hydrogen bond in the ordered solution conformation is probably either the backbone carbonyl oxygen of asparagine (as in the crystal structures, Figure 2, A and B) or the asparagine side-chain carbonyl oxygen. Either model is consistent with the NOE measurements in H_2O, described above, and the Raman spectroscopic data which show that some fraction of the conformational ensemble in H_2O has similar (but not identical) amide III vibrational frequencies as the type I β-bend conformation of the solid state.

It is interesting to note that, because of its electron-withdrawing effect, hydrogen bonding to the asparagine side-chain carbonyl is expected to *increase* the rate of base-catalyzed side-chain amide proton exchange. Hence, the somewhat faster side-chain amide proton exchange rates observed for *trans*-Ac-Asn-Pro-Tyr-NHMe (Table IV) *may* reflect a hydrogen bond between the side-chain carbonyl oxygen and the Tyr NH (as in the crystal structure) or NHMe backbone amide protons.

Conformational free energy calculations, presented in the following paper,[22] indicate that low-energy β-bends at Pro-Tyr of *trans*-Ac-Asn-Pro-Tyr-NHMe are stabilized by hydrogen bonds between the Pro-Tyr-NHMe backbone and the Asn side chain. This conclusion is consistent with the X-ray crystal structure in which the Tyr NH amide proton is intramolecularly hydrogen bonded to the Asn side-chain carbonyl oxygen in a type I (at Pro-Tyr) β-bend conformation. A role for the Asn side chain in stabilizing β-bends at Pro-Tyr is also consistent with our study in aqueous solution. NOE measurements indicate a population of conformers in which the Asn CONH^2 side-chain amide proton is near the NHMe amide proton, while saturation transfer measurements indicate a significant fraction of molecules with hydrogen bonds involving the Tyr NH and NHMe amide protons. The enhanced rate of exchange observed for the Asn side-chain amide protons, as pointed out above, *may* indicate that this side-chain carbonyl oxygen is a hydrogen-bond acceptor. In addition, *trans*-Ac-Pro-Tyr-NHMe, which lacks the potential for β-bend stabilization by the Asn side chain, did not exhibit unusually slow amide proton exchange rates, indicating little or no hydrogen-bonded β-bend conformation.

Taken together, the data in H_2O indicate that the predominant conformation (~50%) of Ac-Asn-Pro-Tyr-NHMe in solution has an intramolecularly hydrogen-bonded β-bend at Pro-Tyr (probably type I), with a *trans*-Asn-Pro peptide bond. The NMR measurements, however, were not able to identify the conformational features in solution which give rise to the ~1380-cm^{-1} deuterium-sensitive Raman mode in water. Although many spectroscopic features indicate that the predominant solution conformation is similar to the type I β-bend conformation of the solid state, the ~1380-cm^{-1} band is replaced by a weak ~1370-cm^{-1} band in the solid-state spectrum. Hence, the frequency and intensity of this mode appear to be very sensitive to the molecular conformation or solvation state of the peptide.

Conformational Analysis of Ac-Tyr-Pro-Asn-NHMe. In the solid state, Ac-Tyr-Pro-Asn-NHMe has an extended backbone conformation, with all *trans*-peptide bonds. While the conformation which crystallizes out of solution is not a β-bend, a 180° variation of ϕ_{Asn} (−88° in the crystal structure) would yield a conformation close to the type II bend of the Tyr-Pro-Asn sequence in concanavalin A (cf. Table II). Similarly, a change of ψ_{Pro} from 141° in this tripeptide crystal structure to −30° would generate a type I β-bend. Intermolecular interactions in the solid state need affect only one dihedral angle to convert a β-bend solution conformation to an extended solid-state conformation. Similar observations have been made for the crystal structure[84] of Tyr-Pro-Asn-Gly, which also has an extended backbone conformation.

The solution structure determination of Ac-Tyr-Pro-Asn-NHMe was hindered by solubility problems encountered above 10 mg/mL. Measurements made at <5 mg/mL demonstrate the presence of several minor conformations detected by the tyrosine ring resonance splitting pattern (unpublished results). At low peptide concentrations, the backbone amide exchange rate constant for the NHMe amide proton of *trans*-Ac-Tyr-Pro-Asn-NHMe is slower (rather than faster) than that of Ac-Asn-NHMe, indicating a population of *trans*-Ac-Tyr-Pro-Asn-NHMe molecules in which this amide proton is hydrogen bonded. No evidence for hydrogen bonding was observed in the other amide protons of *trans*-Ac-Tyr-Pro-Asn-NHMe. This same backbone hydrogen bond was identified in Me_2SO solutions (unpublished results). While the experimental data indicate the presence of a population of hydrogen-bonded species, the identification of a backbone hydrogen bond does not provide sufficient conformational constraints to determine the dominant solution structure in water.

A summary of the combined experimental and theoretical conformational analysis of Ac-Asn-Pro-Tyr-NHMe and Ac-Tyr-Pro-Asn-NHMe is presented in the following paper.[22]

The Unreliability of the Tyr Fermi Resonance Doublet in Assigning Phenolic Hydrogen Bonds. The strong doublet at ~850 and 830 cm^{-1} in the Raman spectra of Tyr-containing polypeptides has been assigned[76] to Fermi resonance between the ring-breathing vibration and the overtone of an out-of-plane ring-bending mode of para-substituted benzenes. Empirically, the intensity ratio of this doublet is correlated with the hydrogen-bonding environment and state of ionization of the phenolic hydroxyl group and is otherwise independent of the environment of the phenyl ring or the conformation of the backbone. When Tyr acts as a hydrogen bond acceptor, or donor, the I_{850}/I_{830} ratio ranges from 1.4 to 2.5 or 0.3 to 0.9, respectively.

In the crystalline state, Ac-Asn-Pro-Tyr-NHMe has an intensity ratio I_{850}/I_{830} of 1.55, which according to this interpretation indicates that the Tyr OH is a weak hydrogen bond acceptor in the solid state. The crystal data for Ac-Asn-Pro-Tyr-NHMe form I (crystallized from water) do not support this assignment, since the phenolic hydroxyl group is involved as an intermolecular hydrogen bond donor to the tyrosine backbone carbonyl oxygen

(83) Billeter, M.; Braun, W.; Wüthrich, K. *J. Mol. Biol.* **1982**, *155*, 321.

(84) Prēcigoux, G.; Geoffre, S.; Hospital, M.; Leroy, F. *Acta Crystallog., Sect. B* **1982**, *B38*, 2172.

(Tyr $O^{\eta}H$···O-Tyr, with an oxygen/oxygen interatomic distance of 2.67 Å). The closest potential hydrogen bond donors in the crystal structure (Asn CONH^2 and Asn $N^{\alpha}H$, which can also form intermolecular hydrogen bonds) are greater than 3.5 Å (nitrogen/oxygen interatomic distance) away. These results suggest caution in the interpretation of the relative intensities of the tyrosine doublet due to Fermi resonance in solution Raman spectra.

Role of β-Bend Conformations of Asn-Pro-Tyr and Tyr-Pro-Asn in the Folding Mechanism of Disulfide-Intact Ribonuclease A. It is important to recognize that partially (or incorrectly) folded molecules, or ordered peptide fragments, detected in equilibrium measurements *may* not play a role in the folding mechanism. As has been pointed out elsewhere,[85] the dominant folding mechanism(s) for a particular protein corresponds to the isothermal folding pathway(s) of lowest free energy of activation. This implies that folding intermediates observed in kinetic measurements provide correct information about the folding mechanism(s) and that the conformers detected in equilibrium measurements *may* be unimportant in the predominant folding mechanism.

In this and the following[22] paper, we have examined the conformations which are defined by local interactions at the β-bends of proposed initiation sites[9] E and F (Figure 1) under folding conditions. It is our *assumption* that these rapidly forming (i.e., short-lifetime) structures, defined by short- and medium-range interactions under folding conditions, correspond to structures which form initially in folding intermediates. Having developed a spectroscopic characterization of the bend conformation(s) of *trans*-Ac-Asn-Pro-Tyr-NHMe, it remains to be shown that these structures actually take part in the folding mechanism.

In our view, which is an elaboration of the basic model of Tanaka & Scheraga,[6,7,9] the isothermal folding of ribonuclease A can be considered in three stages, each of which may involve one or more metastable intermediates. In the *initial stage*, short- and medium-range interactions dominate in rapidly establishing one or more local conformations along the chain, referred to here as chain-folding initiation structures, at sequences corresponding to chain-folding initiation sites. Among the ensemble of structures accessible to the unfolded chain (under folding conditions), we assume that particular conformations of certain sequences are strongly favored by local interactions and play a role in the folding mechanism. These local structures limit the conformational space accessible to the protein in the initial stage of folding, thereby directing subsequent folding events. Their formation (or nucleation) need not correspond to the rate-limiting step in folding. A discussion of the location and conformations of likely chain-folding initiation structures in ribonucleases A is presented in the next section.

In the next *intermediate stage* of folding, medium- and long-range interactions dominate as chain-folding initiation structures coalesce into more ordered folding intermediates and, eventually, native-like, predominantly folded structures by growth-merge[7,86] and/or diffusion-collision[87,88] type mechanisms. It should be noted that, in their original context, these two terms referred to the interaction of unstable, transient "microdomains" or "embryos" (which do not correspond to local free energy minima), while here they refer to the interaction of metastable chain-folding initiation structures (corresponding to local free energy minima). Events occurring in this intermediate stage of folding, in which independent chain-folding initiation structures must find and properly orient with one another, are likely to correspond to the rate-limiting step in folding to a native-like structure.

In the *final stage* of folding, local conformational changes and conformational rearrangements take place as the structure settles into the global conformational energy minimum. This *final stage* has been incorporated to account for conformational rearrangement[89] (e.g., proline peptide bond isomerization[90] and rearrangement of hydrophobic clusters[8]) in light of recent evidence[37-42] indicating that ribonuclease A can fold to a native-like "conformationally folded" intermediate before undergoing structural isomerization.

With regard to the folding kinetics of the disulfide-intact protein following a solvent jump to folding conditions, it should be recognized that the rate of proline isomerization will be slow compared to the rate of formation of locally stabilized chain-folding initiation structures. The slow isomerization of X-Pro peptide bonds is a mechanism of kinetic control which determines the fraction of molecules which fold with *cis*- and *trans*-X-Pro peptide bonds under folding conditions. For this reason, the ratio of molecules which initiate folding with *cis*- and *trans*-Asn^{113}-Pro^{114} peptide bonds will be determined by the Pro^{114} *cis/trans* ratio under *denaturing conditions*. These populations correspond to molecules folding on different folding pathways. The conformational analysis presented here, and in the following paper,[22] indicates that, within the ensemble of molecules which fold with *trans*-Pro^{114}, local interactions will favor β-bend formation at Pro^{114}-Tyr^{115}. In the ensemble of molecules which fold with *cis*-Pro^{114}, however, the bend is predicted[22] to form at Asn^{113}-Pro^{114}. Similarly, molecules folding with *cis*-Pro^{93} are predicted[22] to form bends at Tyr^{92}-Pro^{93}.

Location and Conformations of Chain-Folding Initiation Structures in Ribonuclease A: The Multiple Initiation Site Mechanism. Assuming that local conformations stabilized by short- and medium-range interactions form before those which involve long-range interactions, the contact map[9] of ribonuclease A has been used to identify likely candidates for chain-folding initiation sites. These sequences are residues 4–11 (site A), 25–34 (site B), 51–57 (site C), 53–79 (site D), 71–111 (site E), and 103–124 (site F). While chain-folding initiation sequences which have non-native conformations in the initial stage of folding may be overlooked by this technique, these predictions are helpful in designing experimental approaches to identify chain-folding initiation sites. Conformational free energy calculations also identify residues 106–118 (i.e., site F) as the most energetically favorable local "hydrophobic pocket" structure.[8]

In this study, we have found that local interactions in the Asn^{113}-Pro^{114}-Tyr^{115} sequence (within site F) have an intrinsic tendency to form hydrogen-bonded β-bend structures with *trans*-X-Pro peptide bonds in water. Similar conclusions were drawn from conformational energy calculations in the absence of solvent.[22] In addition, conformational energy calculations[22] indicate a very high bend probability (>95%) at X-Pro of Tyr^{92}-Pro^{93}-Asn^{94} (in site E) and Asn^{113}-Pro^{114}-Tyr^{115} (in site F) when the X-Pro peptide bond is *cis*.

Other studies of peptide fragments of ribonuclease A show that early forming local structures may also arise at the N-terminus of the molecule, in site A. Spectroscopic studies[17-20,91] of the C- and S-peptide fragments of ribonuclease A (corresponding to residues 1–13 and 1–20, respectively), both of which include chain-folding initiation site A (residues 4–11), demonstrate that local interactions at low temperatures stabilize a native-like α-helical conformation in this sequence as well. NMR studies of reduced, cysteine S-sulfonated ribonuclease A[17] also demonstrate the presence of local structure involving His-12 under folding conditions. Together with the results presented here, these data indicate that short- and medium-range interactions favor local structure in both the N- and C-terminal regions of ribonuclease, and suggest that chain-folding initiation can take place independently in sites A and F. This multiple initiation site mechanism is especially reasonable in view of the fact that while S-peptide alone is a stable helix at low temperatures, the S-protein (corresponding to the rest of molecule) can also be unfolded reversibly.[92] This demonstrates that these two parts of the molecule can fold independently. Recent studies[93] indicate, however, that

(85) Konishi, Y.; Ooi, T.; Scheraga, H. A. *Biochemistry* **1982**, *21*, 4741.
(86) Gō, N.; Abe, H. *Biopolymers* **1981**, *20*, 991.
(87) Karplus, M.; Weaver, D. L. *Nature (London)* **1976**, *260*, 404.
(88) Karplus, M.; Weaver, D. L. *Biopolymers* **1979**, *18*, 1421.
(89) Konishi, Y.; Ooi, T.; Scheraga, H. A. *Proc. Natl. Acad. Sci. U.S.A.* **1982**, *79*, 5734.
(90) Brandts, J. F.; Halvorson, H. R.; Brennan, M. *Biochemistry* **1975**, *14*, 4953.
(91) Bierzynski, A.; Baldwin, R. L. *J. Mol. Biol.* **1982**, *162*, 173.
(92) Labhardt, A. M.; Baldwin, R. L. *J. Mol. Biol.* **1979**, *135*, 231.

local helical structure in site A does not take part in the rate-limiting step in folding disulfide-intact ribonuclease. It is important to realize that, in a multiple-initiation-site mechanism, local structures in these sequences can play an essential role in the folding mechanism without contributing to the rate-limiting step if they interact with the rest of the (partially folded) protein subsequent to the rate-limiting step. From the existing evidence for a multiple initiation site mechanism, however, we cannot distinguish the model in which chain-folding initiation takes place simultaneously at several sites in the same molecule from an alternative model in which different populations initiate folding at different sites, hence following different folding pathways.

Experimental evidence for independent chain-folding initiation in sites E and F exists in the literature. Immunochemical studies[14,24] demonstrate that of the antigenic sites present in ribonuclease A (viz., residues 1–10, 63–75, and 87–104), the first to fold kinetically is 87–104. This antigenic site corresponds to (most of) chain-folding initiation site E (Figure 1) containing Tyr^{92}-Pro^{93}-Asn^{94}. These immunochemical data were originally interpreted[14,24] as evidence for chain-folding initiation in residues 106–124 which, accordingly, would induce folding in 87–104. This mechanism is not energetically reasonable, since it requires that the few (native) contacts between 106–124 and 87–104 provide sufficient stabilization enthalpy to overcome the loss in entropy which accompanies the formation of a reverse-turn loop at 87–104 (Figure 1). Taken together, the results presented here and in the accompanying paper[22] show that the local interactions present in the isolated Asn^{113}-Pro^{114}-Tyr^{115} (with *cis*- or *trans*-Asn-Pro peptide bonds) and Tyr^{92}-Pro^{93}-Asn^{94} (with *cis*-Tyr-Pro peptide bonds) sequences are sufficient to define independent local β-bend structures within sites E and F. These results also indicate that, until the stage where long-range interactions begin to favor the *cis*-proline conformation, non-native *trans*-peptide bonds at Pro^{114} may be anticipated in ribonuclease folding intermediates containing native-like β-sheet structures. Accordingly, an alternative interpretation of the immunochemical data is that chain-folding initiation takes place *independently* in sites E and F. Since site F is not an antigenic site in the native protein, site E was identified as the first to fold.

Further evidence for independent chain-folding initiation in sequences containing Tyr^{92}-Pro^{93}-Asn^{94} (i.e., site E) and Asn^{113}-Pro^{114}-Tyr^{115} (i.e., site F) comes from an examination of homologous sequences of mammalian pancreatic ribonucleases.[94] Because chain-folding initiation structures are presumed to play an important role in the folding process by limiting the conformational space accessible to the protein in the *initial stage* of folding, sequences corresponding to chain-folding initiation sites should be evolutionarily conserved (although substitutions of physically similar amino acids should be tolerated). Among the 37 homologous mammalian pancreatic ribonucleases for which amino acid sequence data are available, 11 of 22 amino acids in site F (103–124) and 14 of 32 in site E (71–102) are strictly conserved (no variations are observed). Variations which do occur are clustered at the edges of these initiation sites. The sequence Tyr^{92}-Pro^{93}-Asn^{94} is identical in all species. While Pro^{114} is also strictly conserved, substitutions at both Asn^{113} (which can be Asp, Ser, Lys, or Gln) and Tyr^{115} (which can be Pro, Phe, or Ser) are observed. The effect of some of these substitutions on the bend-forming character of the sequence has been addressed theoretically.[22,41] The observed variations (and especially the requirement for Pro) suggest that the general β-bend-forming tendency of the sequence has been selected for.

Role of Local Structures in Oxidative Folding. Chain-folding initiation structures are local conformations which do not, in general, require disulfide bond formation for stability. This conclusion is supported by the fact that reduced ribonuclease retains small amounts of native antigenicity[14] and enzymatic activity.[13] Disulfide bond formation is not required for folding (to a small extent). The native disulfide bond arrangement, however, obviously stabilizes the native conformation(s).

While chain-folding initiation structures are expected to form in the absence of disulfide bonds, the energetics of disulfide-bond and local-structure formation may sometimes be coupled. Chain-folding initiation structures can provide an enthalpic contribution which, along with entropic considerations, determines the distribution of disulfide pairings among oxidative folding intermediates. On the other hand, the stability of the chain-folding initiation structure itself may be enhanced by medium-range disulfide bonds that flank β-bends in chain-folding initiation sites. This situation may occur in ribonuclease A, where the disulfide bond Cys^{64}-Cys^{72} can play a role in stabilizing the β-bend (at Lys^{65}-Asn^{66}) of initiation site D. Non-native disulfide bonds, which later rearrange to the native disulfide pairings, may also catalyze folding in this way.

In addition to suggesting that other synthetic or proteolytic fragments of ribonuclease may exhibit significant amounts of ordered structure in water, the implications of this study are that the reduced protein *under folding conditions* will have local sequences which are partially ordered under conditions of temperature and solution composition for which the native protein conformation is thermodynamically stable. Experiments designed to identify these local structures and their role in the folding mechanism are currently under development in our laboratory.[17]

Acknowledgment. This work was supported by research grants from the National Institute of General Medical Sciences (GM-24893) of the National Institutes of Health, U.S. Public Health Service, from the National Science Foundation (PCM79-20279), and from the National Foundation for Cancer Research. Both G.T.M. and E.A. acknowledge the support of National Science Foundation Predoctoral Fellowships. The authors thank T. Klein for synthesizing several peptides used in this study, S. Rumsey for help with the molecular graphics, and H. C. Marsh, Jr., E. Czurylo, Y. Konishi, S. Lin, C. A. McWherter, F. Ni, J. K. Swadesh, and T. W. Thannhauser for helpful discussions and comments on the manuscript.

Supplementary Material Available: Tables of fractional coordinates and thermal parameters, interatomic bond distances, bond angles, torsional angles, distances for hydrogen bonds and heteroatom contacts, and observed and calculated structure factor magnitudes and calculated phase angles for each crystal structure (63 pages). Ordering information is given on any current masthead page.

(93) Lynn, R. M.; Konishi, Y.; Scheraga, H. A. *Biochemistry* **1984**, *23*, 2470.

(94) Blackburn, P.; Moore, S. In "The Enzymes"; Boyer, P. D., Ed.; Academic Press: New York, 1982; Vol. XV, p 317.